TABLE 1. Pearson's correlation index analysis of Sia-related genes[a]

Index	P value	Gene name	Encoded enzyme
0.937	5.87E-3	ST6GAL1	ST6Gal I
0.806	5.30E-2	ST3GAL3	ST3Gal III
0.551	2.57E-1	CMAH	Pseudogene for CMP-Neu5Ac hydroxylase
0.473	3.44E-1	ST3GAL2	ST3Gal II
0.215	6.82E-1	SLC35A1	CMP-Sia transporter
0.173	7.43E-1	ST8SIA1	ST8Sia I
0.142	7.89E-1	ST3GAL6	ST3Gal VI
0.137	7.96E-1	PGM3	GlcNAc-6-P mutase
0.096	8.56E-1	GMPPB	GDP-Man pyrophosphorylase
0.052	9.22E-1	ST6GALNAC2	ST6GalNAc II
−0.103	8.47E-1	ST8SIA3	ST8Sia III
−0.196	7.10E-1	ST8SIA4	ST8Sia IV/PST
−0.210	6.89E-1	GNE	UDP-GlcNAc-2-epimerase/ManNAc kinase
−0.283	5.87E-1	ST6GALNAC6	ST6GalNAc VI
−0.442	3.80E-1	ST3GAL5	ST3Gal V
−0.448	3.72E-1	ST6GALNAC1	ST6GalNAc I
−0.452	3.68E-1	ST8SIA5	ST8Sia V
−0.508	3.04E-1	SAS	Neu5Ac-9-P synthase
−0.639	1.72E-1	ST6GALNAC4	ST6GalNAc IV
−0.678	1.39E-1	NEU3	Membrane sialidase
−0.696	1.25E-1	NEU1	Lysosomal sialidase
−0.739	9.30E-2	ST8SIA2	ST8Sia II/STX
−0.742	9.12E-2	ST3GAL4	ST3Gal IV
−0.898	1.52E-2	ST3GAL1	ST3Gal I
−0.938	5.62E-3	SIAE	Sia-9-O-acetylesterase

[a] Pearson's correlation coefficient (index) values of relative gene expression in the microarray against relative GL7 staining MFI among six B-cell lines were calculated for sialyltransferase genes and Sia metabolism-related genes. A positive value indicates the presence of a correlation between gene expression and staining. A negative value indicates the presence of a negative correlation. Index values are also expressed as P values.

on *ST6GAL1* expression. To evaluate these findings, we explored the ST6GAL1 expression dependence of GL7 epitope expression. CHO-K1 cells are known to lack α2,6-linked Sia on their cell surfaces. As expected, the parental CHO-K1 cells were GL7 negative (data not shown), as were vector-transfected CHO-K1 cells (Fig. 2B). In contrast, rat *ST6GAL1* (r*St6gal1*)-transfected CHO-K1 cells showed a marked increase in GL7 staining (Fig. 2B). The increase in GL7 staining upon r*St6gal1* expression coincided with the increase in staining by SSA, a plant lectin which reacts with Sia α2,6-Gal/GalNAc on glycans. As CHO-K1 cells are nonimmune cells, GL7 seemed to recognize α2,6-linked Neu5Ac-containing sugar chains on various proteins. Immunoblotting analysis of these stable clones further clarified that the introduction of r*St6gal1* was sufficient to give rise to bands on the blot. The membrane fractions of both CHO-K1 stable clones and human B-cell lines resulted in multiple bands (data not shown).

Glycan-binding assay of GL7. To confirm that GL7 is an antiglycan antibody that recognizes α2,6-linked Sia and also to determine the fine specificity of the epitope, we examined GL7 binding to various glycan probes (65) by ELISA. GL7 bound to LSTc (Neu5Acα2-6Galβ1-4GlcNAcβ1-3Galβ1-4Glc) but not to its structural isomer with α2-3 linked Neu5Ac, LSTa (Neu5Acα2-3Galβ1-3GlcNAcβ1-3Galβ1-4Glc) (Fig. 2C). Interestingly, GL7 did not bind to Neu5Acα2-6Galβ1-4Glc (sialyllactose) in spite of the existence of α2,6-linked Neu5Ac in the probe. The glucose (Glc) of the reducing terminal was destroyed during probe preparation for coupling with strepta-

vidin. Thus, it is likely that the structure of Neu5Acα2-6Gal is not sufficient for GL7 binding but that the binding requires at least a trisaccharide for optimal recognition or GlcNAc in the underlying lactosamine. Taking all of the results into consideration, we concluded that GL7 recognizes α2,6-linked Sia-containing glycan chains that are often found on N-glycans of various proteins.

A shift in the major Sia species, Neu5Gc to Neu5Ac, in the mouse germinal center reaction. It was still not clear why GL7 failed to react with mouse mature B cells, given that these cells abundantly express α2,6-linked sialoglycans, as St6gal1 is also expressed in these cells (20, 64). The dominant difference in sialylation between mice and humans occurs in the Sia modification at the C-5 position (60). Humans predominantly express Neu5Ac, whereas the major Sia in mice is Neu5Gc (Fig. 3A). It is possible that the change in GL7 reactivity could be a consequence of the change in sia modification. Neu5Gc modification in biosynthesis is regulated by the Cmah reaction in the cytosol, which metabolically gives rise to the donor, CMP-Neu5Gc, for a subsequent sialyltransferase reaction(s) in the Golgi apparatus (Fig. 3B) (24, 25). We therefore asked whether mouse B cells undergo a change in Sia species, from Neu5Gc to Neu5Ac, in GL7-positive cells. We first stained the germinal centers with GL7 and the lectin domain of mouse CD22 (mCD22-Fc), because mouse CD22 demonstrates a marked preference for Neu5Gc-bearing over Neu5Ac-bearing α2,6-linked sialoglycan ligands (26, 44, 50). As shown in Fig. 3C, in the SRBC-immunized mouse spleen, GL7-positive germinal centers were specifically excluded by mCD22-Fc recognition. This complementarity of staining appeared to be the result of the probe preferences, Neu5Ac for GL7 and Neu5Gc for mCD22-Fc, respectively. We then assessed Cmah expression and the Neu5Ac-Neu5Gc ratio in GL7-positive germinal center B cells. Germinal center (GL7-bound) cells showed severely reduced expression of Cmah, and this reduction coincided with the loss of Neu5Gc in the membrane fraction of the cells (Fig. 3D). In contrast, GL7-negative SRBC-immunized B cells were not significantly different from nonimmunized splenic B cells. Thus, the gain of GL7 staining reflected the loss of the CD22 ligand in germinal center B cells due to the repression of Cmah.

Real-time PCR analysis during mouse B cell activation. LPS stimulation induces the GL7 epitope in B cells (28). Therefore, we adopted this system to assess the enzyme (gene) responsible for GL7 epitope expression. Cmah is responsible for Sia species change, and St6Gal1 is responsible for Sia linkage biosynthesis. We examined the expression of *Cmah* and *St6gall* to determine whether changes in the expression of these genes could account for the GL7 epitope induction detected in B-cell activation events. In real-time RT-PCR experiments, Cmah expression showed an 80% reduction in LPS-stimulated B cells compared with unstimulated splenic B cells after 48 h of incubation (Fig. 4A). This reduction was already detectable after 3 h of culture. Despite the slightly enhanced expression level of α2,6-linked Sia-containing glycan probed with SSA, *St6gall* expression showed a subtle reduction in activated B cells after 48 h (Fig. 4A and B). *Cmah* reduction appears to play a prominent role in the appearance of the GL7 epitope in activated B cells. Retrovirus-mediated ectopic *Cmah* expression consistently reduced the expression of the GL7 epitope in
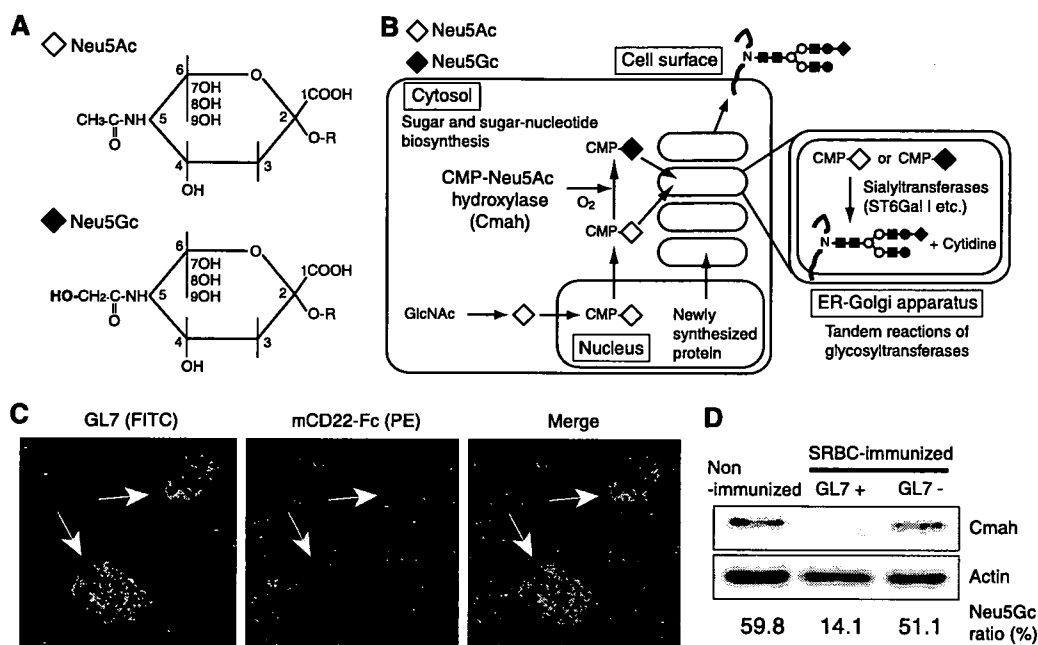
FIG. 3. Change in Sia species in germinal centers. (A) Structural differences between two major molecular species of Sia. The metabolic precursor Neu5Ac and its modified form Neu5Gc differ only by an oxygen atom at the C-5 position. The conversion of CMP-Neu5Ac to CMP-Neu5Gc is catalyzed by the enzyme Cmah. (B) Biosynthesis of sialylated glycoproteins destined for the cell surface. Cytosolic metabolism of Sia is responsible for the abundance of the molecular species of Sia on the cell surface, as a given ratio of cytosolic CMP-Sia is imported into the Golgi apparatus and then used by the sialyltransferases for the biosynthesis of glycoproteins en route to the plasma membrane. (C) Loss of CD22 ligand in germinal centers. Spleen sections of SRBC-immunized mice (10 days after immunization) were costained with FITC-conjugated GL7 and mCD22-Fc precomplexed with R-PE-conjugated anti-human IgG. The mCD22-Fc is a chimeric probe that binds to the CD22 ligand. Arrows indicate germinal centers. (D) Downregulation of Cmah expression in germinal center B cells. GL7-positive germinal center cells and GL7-negative cells were prepared from a B-cell-enriched fraction derived from the spleen of a mouse 12 days after immunization with SRBC. Ultracentrifugation supernatant fractions (cytosolic fractions) of untreated mouse B cells (nonimmunized; control), GL7-positive B cells (GL7+), and GL7-negative B cells (GL7−) were subjected to immunoblotting with anti-mouse Cmah antibody and antiactin antibody (to demonstrate equal loading of samples). The Neu5Gc/(Neu5Ac+Neu5Gc) ratio of the ultracentrifugation pellets (membrane fractions) of each cell type was measured by HPLC.

LPS-stimulated B blasts (Fig. 4C), further confirming the responsibility of *Cmah* for the repression of the appearance of the GL7 epitope. After 48 h of stimulation with LPS, *Gapdh* expression increased by about 30% (Fig. 4A). This may be attributable to the blastic transformation of LPS-stimulated proliferating B cells (B blasts), which produce much more cytosolic space and subsequent metabolism than resting B cells. GL7 staining of LPS-stimulated B cells showed heterogeneity in the degree of staining. Thus, cells used to prepare RNA for this real-time PCR experiment were a mixture of GL7^{high} and GL7^{low} cells. When these finding are taken into consideration, the reduction of *Cmah* expression in GL7^{high} germinal center B cells could be more drastic. The expression of *Cd22*, an α2,6-linked Neu5Gc binding protein, on B cells was reduced to around 40% after 48 h, even though its cell surface expression was still comparable to that of unstimulated cells in flow cytometry (Fig. 4A and B).

Targeted disruption of the Cmah gene in mice. To further examine the in vivo function of Neu5Gc-bearing glycans, we targeted the *Cmah* gene in mice by inserting the neomycin resistance gene cassette into the second coding exon (Fig. 5A and B). Biochemical analysis of mouse tissues made it clear that gene inactivation was achieved, as homozygous null mice lacked enzyme expression in the liver ultracentrifugation su-

pernatant, as shown by immunoblotting using antiserum against the N terminus of Cmah (Fig. 5C). We also did not detect a signal with a different molecular mass from the *Cmah*-disrupted allele. We further analyzed the effect of the enzyme deficiency on the level of its product by HPLC. *Cmah*-null tissues lacked detectable production of Neu5Gc throughout the normal adult mouse body (Fig. 5D). We concluded that the *Cmah* gene is indispensable for most of the cellular biosynthesis of Neu5Gc, as previously suggested in humans (6, 22). The development of the null mice appeared to be grossly normal; however, the numbers of null and heterozygote mutant offspring derived from F_1 crosses were subtly reduced from wild-type littermates in the rate expected from Mendelian rules (wild-type:heterozygote: null, 508:881:449), even though the mice were bred in a specific-pathogen-free mouse facility.

Normal B-cell maturation in Cmah-deficient mice. We found that Neu5Gc expression was severely repressed during B-cell activation in germinal centers, and thus we examined the development of the immune system in *Cmah*-null mice. In null mice, the values from blood counts and blood chemistry analyses were normal in every category examined (white blood cell, red blood cell, blood hemoglobin, hematocrit, mean corpuscular volume, mean corpuscular hemoglobin, mean corpuscular
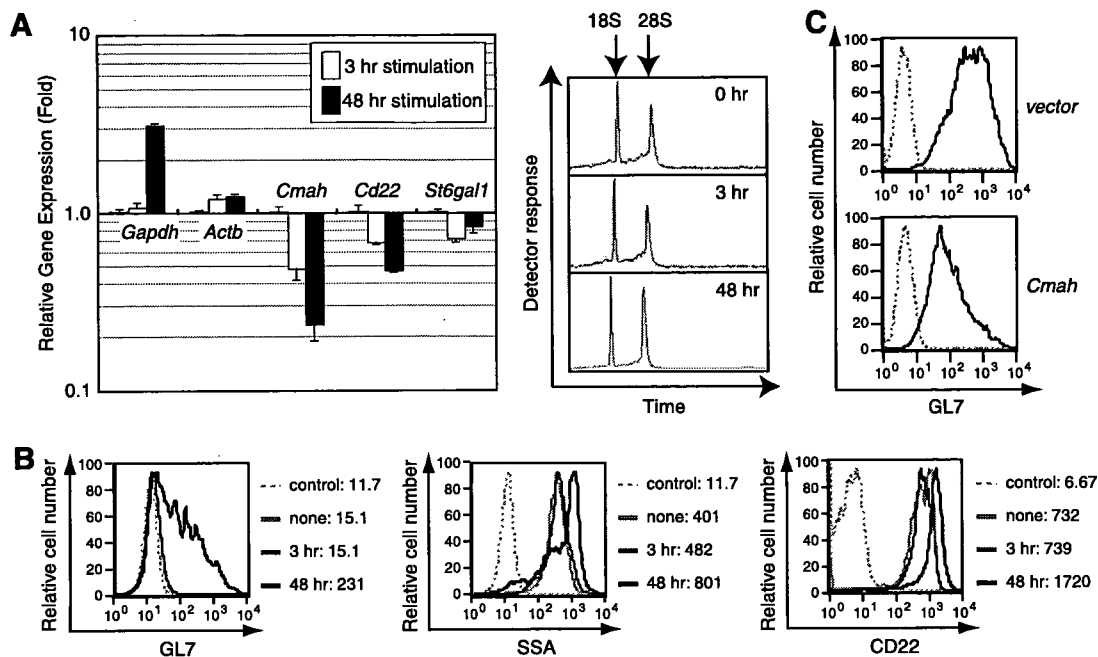
FIG. 4. Downregulation of *Cmah* mRNA in primary cultured B cell blasts, causing GL7 epitope expression. (A and B) Cmah repression caused by in vitro B-cell activation. Splenic B cells were stimulated with 30 μg/ml LPS for the indicated times. Reverse-transcribed cDNAs prepared from total RNA of these cells were subjected to real-time PCR analysis. The right box shows capillary electrophoresis analysis results indicating the lack of RNA degradation in the RNA used for cDNA synthesis. The expression levels of the mRNA of *Gapdh*, *Actb* (beta actin), *Cmah*, *Cd22*, and *St6gal1* are shown as the relative change compared with the mRNA expression in untreated B cells (A). The same set of cells that was used to prepare total RNA was stained with FITC-conjugated GL7, SSA, and anti-CD22 (B). The MFI of each stain is indicated at the right of each panel. (C) Reduced expression of the GL7 epitope by ectopic *Cmah* expression. *Cmah* was ectopically expressed in LPS-stimulated splenic B blasts using retrovirus. Retrovirus-infected cells were sorted and stained with FITC-conjugated GL7.

hemoglobin concentrate, and platelet). The development of immune cells in *Cmah*-null mice appeared to be grossly normal for T-cell and B-cell maturation, as indicated by routine flow cytometric analysis profiles. The indicators analyzed included the ratio of B1 to B2 cells, the ratio of marginal zone to follicular B cells, and the expression level of surface IgM, major histocompatibility complex class II (MHC-II), and CD22 (Fig. 5E; also see Table S2 in the supplemental material). We also examined the staining profile of activation markers for B cells. The only probe with a significant change in the null B cells was GL7 (Fig. 5F), which recognizes α2,6-linked Neu5Ac on LacNAc (Fig. 2C). Serum Ig measurements using the sandwich ELISA method revealed a significant ($P = 0.074$) increase in the serum IgG1 level of the *Cmah*-null population (Table 2).

Hyperreactive B cells in *Cmah*-deficient mice. We examined the mouse phenotype after immunization. When mice were immunized with the T-dependent antigen DNP-KLH or the T-independent (II) antigen DNP-Ficoll, the response to the T-independent antigen (serum titer against the hapten, DNP conjugated to BSA, by ELISA) was enhanced in null mice compared with controls, most prominently for IgM but also significantly for IgG3 (Fig. 6A). In contrast, the T-dependent response of the null group to DNP-KLH with potent complete Freund's adjuvant was not significantly different from that of the control group (Fig. 6B). Thus, the Neu5Gc deficiency in B cells resulted in a hyperresponsive phenotype to the T-independent antigen, indicating the importance of Neu5Gc-mediated negative regulation of B-cell activation. To further study

the regulatory mechanism of the B-cell response by Neu5Gc-bearing glycans, mature splenic B cells were isolated and used in an in vitro proliferation assay with various stimuli. In this assay, compared with the cells from littermate controls, *Cmah*-null B cells proliferated robustly in response to the F(ab')₂ fragment against BCR (anti-μ chain), regardless of interleukin-4 (IL-4) addition (Fig. 6C). The FBS routinely used to support the cell culture contains around 5% Neu5Gc and represents a possible supply for *Cmah*-null cells. Therefore, we also examined the difference in proliferation using serum from chickens and humans, which contain only Neu5Ac as a Sia source (as determined by HPLC analysis [data not shown]). Under such conditions, *Cmah*-null B cells also showed augmented proliferation compared with control cells, although the degree of overall proliferation was much stronger in medium with FBS, perhaps because of differences in the growth factor(s) contained in each type of serum (data not shown). When anti-CD40 was used as the stimulus in a model mimicking T-dependent stimulation, B cells with both genotypes proliferated equally (data not shown); thus, Neu5Gc glycan-mediated regulation appeared to be stimulation dependent, and the effect seemed to be more related to T-independent activation. When T-cell proliferation was assessed using anti-CD3 as the stimulant, both *Cmah*-null and control splenic T cells proliferated to the same extent (see Fig. S2A in the supplemental material). No obvious bias toward either Th1 or Th2 was found in the cytokine production pattern of anti-CD3-stimulated *Cmah*-null T cells; however, a significant reduction of gamma
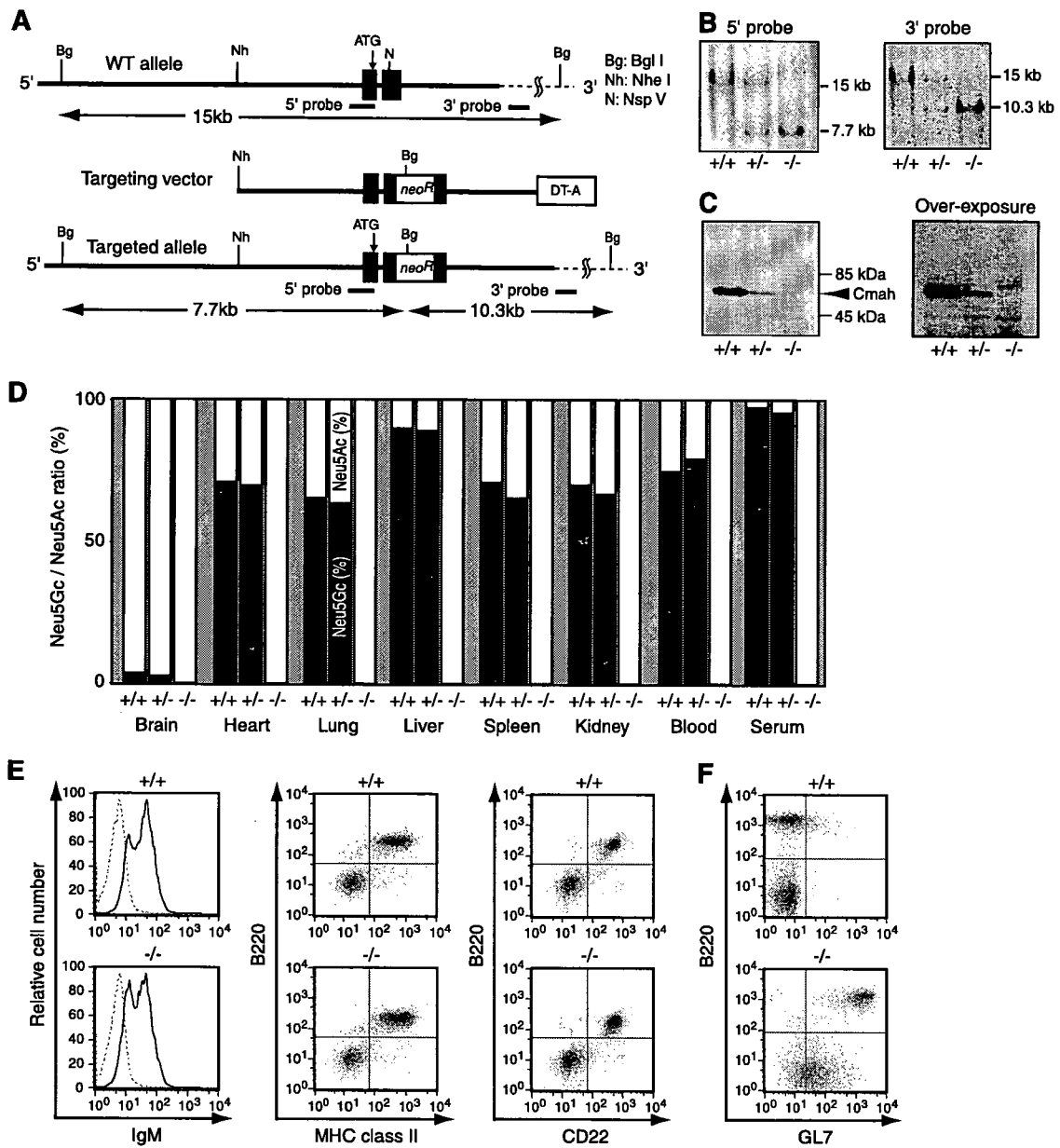
FIG. 5. Generation and biochemical analyses of *Cmah* knockout mice. (A) Allele for targeted *Cmah*. A targeting vector was created by inserting the *PGK-neoR* cassette into the NspV site of the second coding exon (exon 5) of the *Cmah* gene. (B) Genotype of homologous recombination of selected ES cell lines. The genotypes of G418-selected cell lines were determined by Southern blotting analysis of genomic DNA digested with BglI, using both radiolabeled 5′ internal and 3′ external probes. The genetic status of the *Cmah* allele is indicated as follows: +/+, wild type; +/−, heterozygote; and −/−, null (B to F). (C) Loss of Cmah enzyme demonstrated by immunoblotting analysis of liver cytosolic fractions. Ultracentrifugation supernatant fractions of livers were assessed for the expression of Cmah using anti-mouse Cmah immunoblotting. Staining of a ∼67-kDa band (arrowhead) in wild-type and heterozygote livers represents the signal of Cmah, which is not detectable in *Cmah*-null liver samples. (D) Loss of Neu5Gc production throughout the body in mutated mice. Acid-hydrolyzed Sia from the indicated tissues was derivatized using DMB, and the ratios of Neu5Ac and Neu5Gc to total Sia were measured by reverse-phase HPLC. Solid columns represent the percentage of Neu5Gc in various tissues, and open columns represent the percentage of Neu5Ac. The detection limit for Neu5Gc in this assay was around 0.1%. (E) Flow cytometry profile of *Cmah*-null mice splenocytes. The expression of IgM, MHC-II (I-A and I-E), and CD22 on splenocytes from wild-type and *Cmah*-null mice was detected by flow cytometry. In anti-MHC-II and anti-CD22 staining, splenocytes were costained with anti-B220, a marker for B cells. (F) Strong expression of the GL7 epitope on *Cmah*-null mice B cells. Splenocytes from wild-type and *Cmah*-null mice were costained with anti-B220 and GL7 and subjected to flow cytometry.

interferon and IL-4 secretion was found in these cells (see Fig. S2B in the supplemental material). Based on these findings, we conclude that B cells from *Cmah*-deficient mice acquire hyper-responsiveness to stimuli, and thus the null animals show

hyperresponsiveness (hyperproduction of antibodies) to the T-independent antigen.

Retrovirus-mediated rescue of hyperproliferative B-cell response in null mice. The LPS stimulation-dependent prolifer-

TABLE 2. Serum Ig isotype levels of nonimmunized *Cmah*-null mice

Isotype	Serum Ig level (μg/ml)[a]		
	Wild type	Heterozygote	*Cmah* null
IgM	169.6 ± 24.7	205.3 ± 38.9	190.0 ± 33.3
IgG1[b]	115.5 ± 14.9	151.3 ± 19.5	197.4 ± 41.2
IgG3	20.4 ± 2.3	23.9 ± 3.1	19.6 ± 3.8
IgA	242.7 ± 9.7	280.0 ± 29.2	260.2 ± 10.6

[a] Serum Ig levels were measured in nonimmunized mice at 7 to 13 weeks of age (at least 20 per genotype). Values are expressed as the means ± standard errors of the means.

[b] The serum IgG1 level was slightly increased in *Cmah*-null mice (Student's *t* test; $P = 0.074$ for wild type versus *Cmah* null).

ative response is also related to the T-independent response. In *Cmah*-null B cells, LPS stimulation caused enhanced proliferation (Fig. 7A). Given that LPS induces a considerable percentage of cells to progress through the cell cycle, retroviral infection-mediated gene rescue is possible. To determine whether the B-cell hyperreactivity was caused by the *Cmah* mutation, we expressed Cmah ectopically in LPS-stimulated proliferating *Cmah*-null B cells and found that the introduction of *Cmah* did result in repression of the hyperproliferation of *Cmah*-null B cells (Fig. 7B). This rescued hyperproliferative phenotype produced by ectopic Cmah expression in *Cmah*-null B cells indicates that the phenotypes in *Cmah*-null mice are caused by the loss of Cmah expression and probably not by effects on the expression of other genes owing to the insertion of the neomycin-resistance cassette during ES cell-based mutagenesis. This conclusion is also supported by the consistent phenotype resulting from the *Cmah*-disrupted allele in an extensively backcrossed C57BL/6J background. Moreover, our RT-PCR results confirmed equal expression levels of *Lrrc16* and *6330500D04Rik*, the genes located adjacent to the *Cmah* gene in the genome, in splenocytes of wild-type and *Cmah*-null mice (data not shown). To infect control and *Cmah*-encoding retrovirus, we used the same *Cmah*-null B-cell fractions. Since attenuated proliferation was found in *Cmah*-infected B-cell blasts, the augmented proliferation found in the *Cmah*-null B cells compared to the wild type (Fig. 6C) was not due to any subtle population difference in the B-cell fraction. Thus, we conclude that Cmah expression determines the proliferation of B cells when activated and that the difference in the in vivo response to the T-independent antigen is caused by differential expression of Neu5Gc in B cells.

Normal germinal center formation in the Cmah-deficient spleen. As shown in Fig. 5F, *Cmah*-null B cells strongly express the GL7 epitope, and GL7 has been used to detect the germinal center reaction in mice (5, 17, 41, 55). GL7-negative mature B cells turn GL7 positive during germinal center reactions upon T-dependent immunization. Germinal center B cells further develop to CD79b-positive memory B cells, which are no longer stained by GL7 (52). Therefore, it was of interest to assess whether these *Cmah*-null mice could undergo normal germinal center formation. PNA binds to glycan moieties with a terminal β-galactose residue at the core-1 branch of O-linked glycans, and it has been used as a marker for germinal center B cells (8). We compared the staining profiles of the two germinal center probes using spleen sections of wild-type and *Cmah*-null mice, either with or without SRBC immunization.

In the wild-type spleen without immunization, PNA showed some staining in the marginal zone area, whereas GL7 did not (Fig. 8A). As expected from flow cytometric staining, GL7 widely stained the B-cell zone of the *Cmah*-null spleen even without immunization (Fig. 8A). When wild-type mice were immunized with SRBC, in addition to the marginal zone staining, intense PNA-positive germinal center follicles were observed. When PNA and GL7 staining results were compared on merged images, PNA appeared to stain a larger number of cells in the germinal center than did GL7, which stained a limited number of cells in the area, most probably centrocytes (Fig. 8B). In SRBC-immunized *Cmah*-null spleen, the staining pattern of GL7 was not different from that of the nonimmunized spleen section. These results confirmed that the appearance of GL7 epitope via the conversion of Neu5Gc to Neu5Ac is an activation-dependent event in the wild-type spleen, whereas *Cmah*-null mice lose Neu5Gc throughout; thus, *Cmah*-null spleen was stained by GL7 regardless of the immunization. In contrast, with GL7 staining, the *Cmah*-null spleen formed PNA-positive follicles that resembled the germinal centers of wild-type sections (Fig. 8B). These results suggest that *Cmah*-null mice could develop germinal centers upon SRBC immunization, which is consistent with the normal T-dependent antigen response found in *Cmah*-null mice.

Change in ligand expression for Siglecs in Cmah-null mice. The cell surface change in Sia species (Neu5Gc to Neu5Ac) by *Cmah* disruption could potentially cause a global change in sialylated glycan recognition throughout the body, as Neu5Gc is the predominant form of Sia in the mouse body, except in the neural system (Fig. 5D). In the immune system, various members of the Siglec family of Sia-binding lectins are expressed in a variety of immune cells. The counter-receptors for sialylated glycans affected by the C-5 position oxygen atom include sialoadhesin (Siglec-1, or CD169), which requires α2,3-linked Neu5Ac on galactose as a ligand (10), and CD22 (Siglec-2), which has a strong preference for Neu5Gc over Neu5Ac in the α2,6 linkage to LacNAc in mice (3, 26, 44, 50). To explore the change in ligand expression for Siglecs in *Cmah*-null mice, we prepared Siglec-Fc fusion probes that were free from intramolecular sialylation. In null B cells, the expression of the CD22 ligand was reduced roughly 20-fold compared with that in wild-type cells (Fig. 9A). We also histochemically examined the expression of the CD22 ligand on spleen sections from *Cmah*-null mice. Regardless of immunization, the mCD22-Fc probe failed to detect any staining in the sections of *Cmah*-null spleen, as in the germinal centers of immunized wild-type mice (Fig. 9B). Therefore, *Cmah* disruption caused the reduction of the optimal ligand for CD22. At the same time, ligand expression for sialoadhesin was greatly increased in *Cmah*-null mice (Fig. 9A). Sialoadhesin is expressed on macrophages, whereas CD22 is expressed on B cells. Ligand(s) for Siglec-G, another Siglec molecule presumably expressed on B cells, was not detected on B cells (data not shown); thus, the Siglec-related effects in *Cmah*-null B cells could be a loss of CD22 ligand.

Normal tyrosine phosphorylation upon BCR cross-linking in Cmah-null B cells. In addition to its biochemical activity as a lectin, CD22 also contains immunoreceptor tyrosine-based inhibitory motifs (ITIMs) in its cytoplasmic tail (4, 48). These ITIMs are phosphorylated as part of the phosphorylation
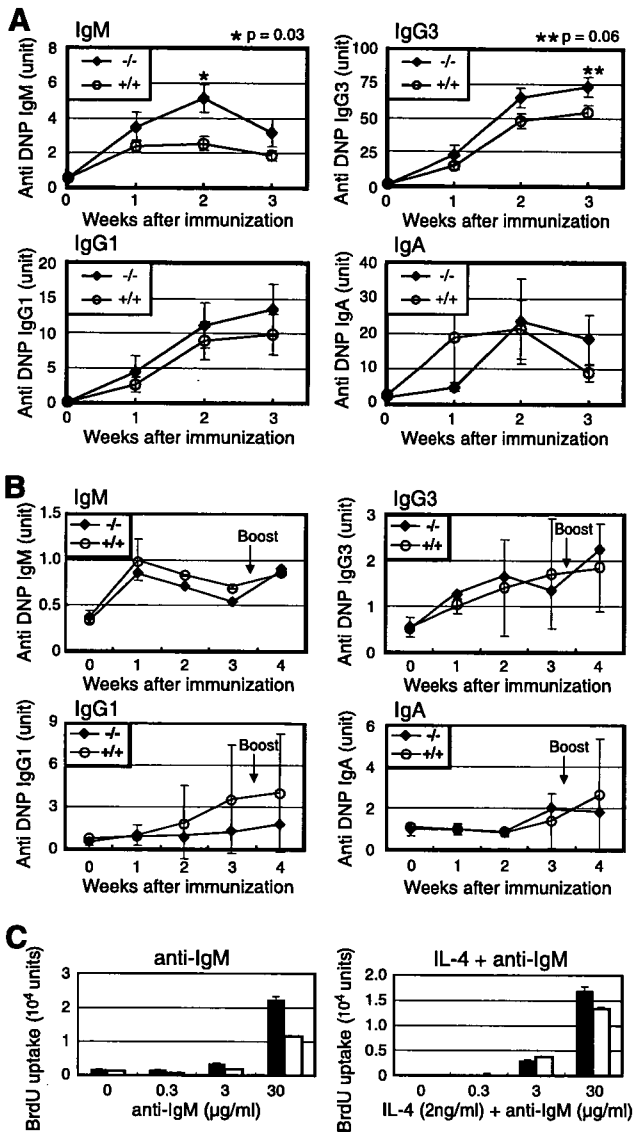
A

B

C

FIG. 6. Hyperresponsive phenotypes of *Cmah*-null mice. (A) T-independent hyperresponse of *Cmah*-null mice. DNP-Ficoll was used to immunize 8-week-old mice. Serum was collected each week and analyzed for reactivity with DNP-conjugated BSA coated on ELISA plates. The titer of hapten-reacting mouse Igs from each animal was determined by isotype-specific ELISA. The measured optical density at 405 nm was normalized to anti-DNP units by comparison with the value from standard pooled serum against DNP on the same plate. The results are presented as the mean responses of 10 animals for each genotype measured in two sets of experiments. The bars represent standard errors of the means. Open circles indicate the responses of wild-type mice, and filled diamonds indicate the responses of *Cmah*-null mice for each isotype. Genotypes are indicated as follows: +/+, wild-type; −/−, *Cmah*-null (A and B). (B) Normal T-dependent immune response of *Cmah*-null mice. DNP-KLH in complete Freund's adjuvant was used to immunize 8-week-old mice. The titers of hapten-reacting mouse Igs from each animal were determined by isotype-specific ELISA as above. Arrows indicate the time of secondary immunization with DNP-KLH. Open circles indicate the responses of wild-type mice, and filled diamonds indicate the responses of *Cmah*-null mice for each isotype. (C) In vitro hyperproliferation response of *Cmah*-null B cells. Splenic B cells from wild-type (open columns) and *Cmah*-null (filled columns) mice were assessed for proliferation using the F(ab′)₂ fragment of anti-mouse IgM (μ chain) or anti-IgM plus
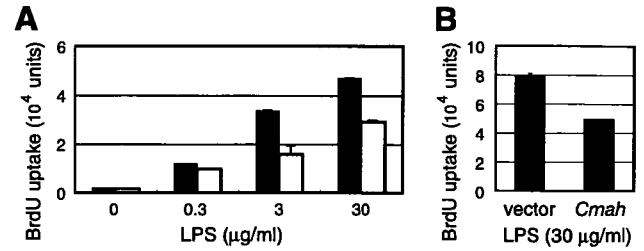
A

B

FIG. 7. Rescue of augmented proliferation of *Cmah*-null B cells by Cmah expression. (A) In vitro hyperproliferation response of *Cmah*-null B cells to LPS. Splenic B cells from wild-type (open columns) and *Cmah*-null mice (filled columns) were assessed for proliferation using LPS from *S. enterica* serovar Enteritidis as the stimulating reagent. Proliferation assays were performed as described in the legend of Fig. 6C. Data are shown as the means of triplicate cultures, and the bars represent standard errors of the means. (B) Reduction of B-cell proliferation by retrovirus-mediated Cmah expression. Cmah was ectopically expressed by mouse stem cell virus in *Cmah*-null splenic LPS B blasts. After being cultured for 2.5 days in the presence of 30 μg/ml LPS, the virus-infected B cells were subjected to a proliferation assay. As a control, cells were infected with an empty vector. Data are shown as the means of triplicate cultures, and the bars represent standard errors of the means.

cascade after BCR cross-linking. CD22 recruits SHP-1 tyrosine phosphatase to negatively regulate BCR signaling (11, 39). Given that CD22 is believed to be a regulator of BCR signaling and B-cell apoptosis (7, 13, 34, 58, 63) and that the level of BCR in *Cmah*-null mice was not different from that of the wild-type control (Fig. 5E), we analyzed the immediate-early CD22 phosphorylation status of mature B cells upon activation by BCR ligation. The overall tyrosine phosphorylation profile of B cells was not different for the two types of mice when the F(ab′)₂ fragment of the anti-IgM (anti-μ chain) was used as a stimulant (Fig. 9C), although this may not be an optimal stimulant for CD22 phosphorylation (21). We further confirmed the tyrosine phosphorylation of CD22, possibly by Lyn kinase at the ITIM motif, upon BCR ligation. Consistently, the phosphorylation profile of CD22 assessed after immunoprecipitation by immunoblotting with an anti-phosphotyrosine antibody was almost identical in *Cmah*-null B cells and controls (Fig. 9D). In contrast, *Cmah*-null B cells showed augmented proliferation when a combination of tetradecanoyl phorbol acetate and ionomycin was used as a stimulant to directly activate classical protein kinase C(s). Thus, a downstream event of protein kinase C activation probably affects the hyperproliferative phenotype of *Cmah*-null B cells (Fig. 9E).

DISCUSSION

Change in Sia species in the germinal center. In the present study, we showed that activated B cells undergo a dramatic
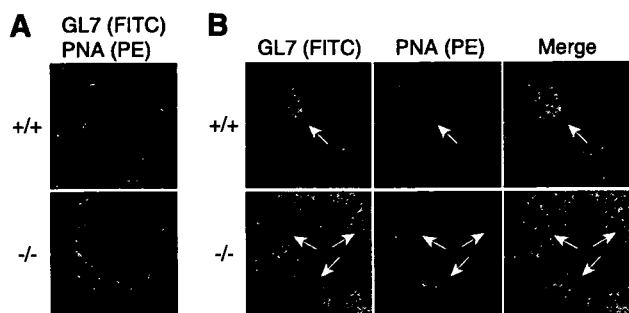
FIG. 8. Changes in staining of germinal center markers in normal or SRBC-immunized Cmah-null mice. (A) Histochemical analyses of spleen sections without immunization. Spleen sections from wild-type and Cmah-null mice were costained with FITC-conjugated GL7 and biotin-conjugated PNA visualized by R-PE-conjugated streptavidin. (B) Histochemical analyses of spleen sections after T-dependent immunization. Wild-type and Cmah-null mice were immunized with SRBC, and the spleens were removed 8 days after immunization. The frozen spleen sections were costained with FITC-conjugated GL7 and biotin-conjugated PNA followed by R-PE-conjugated streptavidin. Arrows indicate germinal centers. Genotypes are indicated as follows: +/+, wild type; −/−, Cmah null.

alteration of surface-sialylated glycans and that this alteration of Sia species from Neu5Gc to Neu5Ac can be probed with GL7. This is the first report regarding the epitope identification of GL7, which is routinely used to stain germinal center B cells in mice. We demonstrated that the GL7 epitope is the Neu5Acα2-6LacNAc-containing N-glycan, which is prominently expressed in activated B cells upon the repression of Cmah. Gain of GL7 epitope expression coincided with the loss of optimal ligand expression of CD22 in germinal center B cells, presumably centrocytes. Considering the rather strong degree of GL7 positivity in germinal center B cells in comparison with in vitro stimulated B-cell blasts, the degree of Cmah reduction might have been severe in these cells. In general, it is thought that Neu5Gc is easy to accumulate but difficult to turn over in cells. This is attributable to the one-way direction of the metabolic pathway; Neu5Gc is biosynthesized by Cmah from Neu5Ac (24, 36, 54), whereas no conversion activity was found to biosynthesize Neu5Ac from Neu5Gc. Therefore, the reduction of Neu5Gc found in the GL7-enriched germinal center cells is remarkable. Such rapid clearance of Neu5Gc could be attributable to several characteristics of germinal center cells. Most importantly, as shown in Fig. 3D, these cells repressed Cmah, the enzyme responsible for the de novo biosynthesis of Neu5Gc. Moreover, because lymphocytes are small cells with limited cytosolic space, the cytosolic pool of Sia in these cells is likely limited and easily turned over. In addition, centrocytes undergo extremely fast cell cycles (66), which probably leads to rapid passive dilution of the cytosolic pool in these cells. At the same time, new protein synthesis should be a primary event that happens in germinal center B cells, as shown by cDNA microarray analysis (51). The transcriptional repression of Cmah, together with these features of germinal center cells, could contribute to the efficient conversion of the major Sia species from Neu5Gc to Neu5Ac.

Negative regulation of B-cell activation by Cmah and its product, Neu5Gc. To clarify the biological role of Neu5Gc in

vivo, we disrupted the Cmah gene in mice and examined their B-cell activation phenotypes. Cmah-null mice showed a hyperreactive B-cell phenotype to T-independent stimulation. In contrast, the T-dependent immunization response was similar to that in wild-type mice. This is consistent with the findings that Cmah expression is severely repressed in the germinal centers of wild-type spleen upon T-dependent immunization and that Cmah-null mice could develop follicles stained with PNA, another marker for germinal centers. Forced expression of Cmah caused repression of the proliferative response of Cmah-null B cells, indicating that Neu5Gc-containing sialoglycan functions to suppress B-cell reactivity though the mechanism is still unknown. This suppression via Neu5Gc-containing sialoglycan appears to be canceled by Cmah repression in germinal center B cells that are "activation committed" or "activation competent." The hyperreactive B-cell phenotypes observed in Cmah-null B cells could mirror differences in cellular reactivity between germinal center and nongerminal center B cells, as indicated by differential cell surface expression of the GL7 epitope (5).

Possible change in sialoglycan-receptor interaction in Cmah-null mice. As Cmah disruption results in a single oxygen atom change in these mice, it is expected that this mutation leaves both the Sia amount and Sia linkage intact in terms of sialoglycans, which could change the stability or turnover of the proteins modified with Sia (14). Although only limited information is available, sialyltransferases that biosynthesize sialylated glycans in the Golgi apparatus do not show strong preferences for CMP-Neu5Ac or CMP-Neu5Gc as substrates (59). When we probed linkage-specific protein sialylation by using α2,6-linked Sia-binding plant lectins such as Sambucus nigra agglutinin, we did not observe a change (data not shown). Thus, the molecular event affected in Cmah-null mice is likely to be lectin recognition of a single oxygen atom on sialoglycans expressed on the cell surface, although a single responsible lectin may not explain the phenotype. One of the candidate lectins as the receptor of sialoglycans is the Siglec family (9, 12, 62), though a yet-to-be-characterized Sia-binding molecule could be affected.

When ligand expression for Siglecs was detected using Siglec-Fc probes, Cmah-null mice lost optimal ligand expression for CD22 (Siglec-2). The ligand function of CD22 in a mouse model has been addressed in two different ways. One study was done using St6gal1-knockout mice (20), and another study analyzed gene-targeted mice expressing mutant CD22 molecules that do not interact with ligands (43). The phenotypes found in Cmah-null mice are considerably different from these two previous studies; therefore, Cmah-null phenotypes might be caused by the combination of loss/gain of a Sia-mediated interaction. Additional studies using a combination of various knockout strains related to sialoglycan recognition are required to address such possibilities.

Apart from the phenotypic contribution of CD22 to the assays in the present study, CD22 ligand expression is not static but is, instead, a regulated event during in vivo B-cell activation. We showed that mCD22-Fc probe staining was downregulated in germinal centers. Moreover, it was reported that in vitro activated human B cells unmask CD22 from a cis-ligand (45). Thus, the regulation of CD22 ligand expression
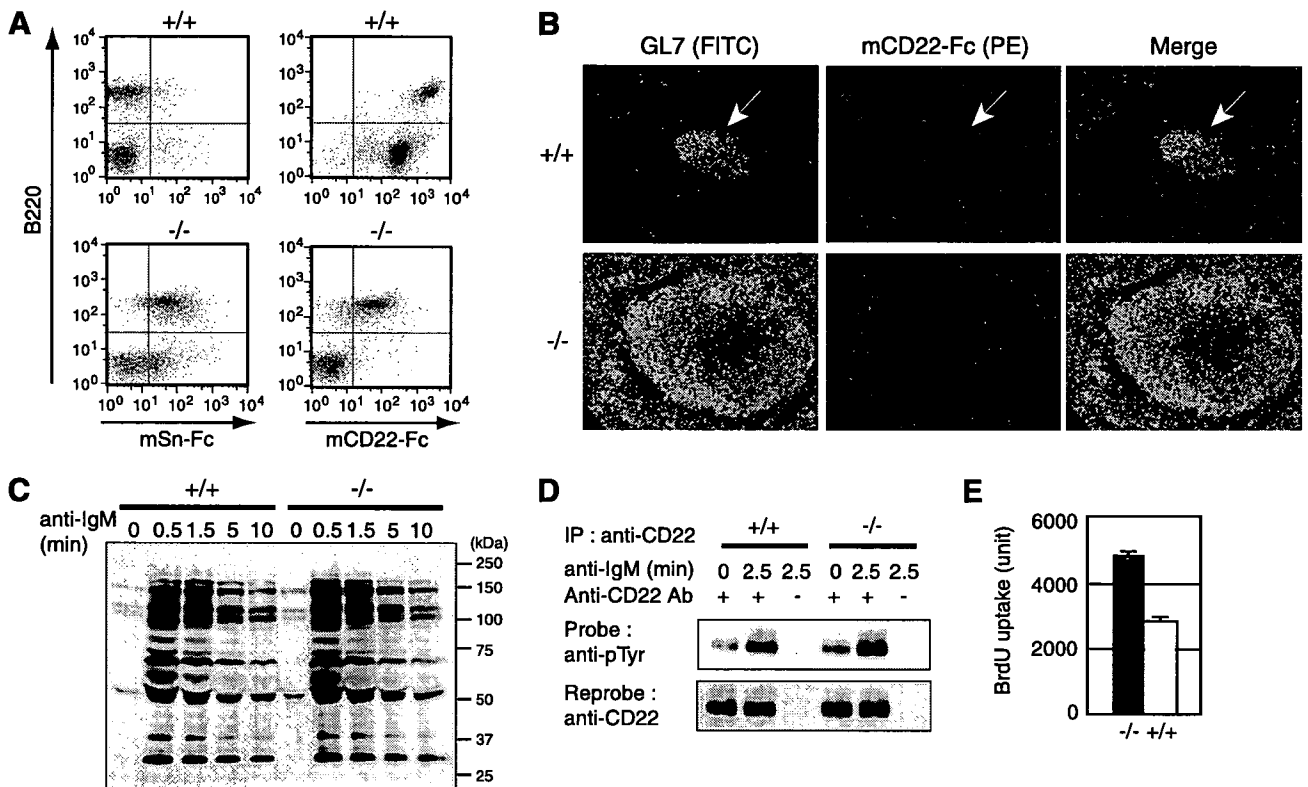
FIG. 9. Loss of optimal CD22 ligand and normal immediate response upon BCR cross-linking in *Cmah*-null mice. (A) Loss of optimal ligand for CD22 in *Cmah*-null mice. The expression of surface ligands for sialoadhesin and CD22 was detected by flow cytometry. Splenocytes from wild-type and *Cmah*-null mice were costained with FITC-conjugated anti-B220 and mSn/mCD22-Fc precomplexed with R-PE-conjugated anti-human IgG. Wild-type B cells were strongly stained with mCD22-Fc. In contrast, the level of mCD22-Fc staining showed a marked decrease in *Cmah*-null mice. The weak signal found on *Cmah*-null splenocytes was detected only with the chimeric probe mCD22-Fc prepared from Lec2 cell culture medium and not with the probe prepared from COS7 cells, possibly because of the autosialy- lation. (B) Histochemical analyses of CD22 ligand expression in spleen sections. Spleen sections from wild-type and *Cmah*-null mice 8 days after SRBC immunization were costained with FITC-conjugated GL7 and mCD22-Fc precomplexed with R-PE-conjugated anti-human IgG. Arrows indicate germinal centers. (C) Overall tyrosine phosphorylation upon anti-IgM stimulation. Splenic B cells from wild-type and *Cmah*-null mice were stimulated with the F(ab')₂ fragment of anti-mouse IgM (μ chain) for the indicated times. Whole-cell lysates were subjected to immunoblotting with antiphosphotyrosine antibody (PT-66). (D) Phosphorylation of CD22. Splenic B cells were stimulated with the F(ab')₂ fragment of anti-mouse IgM (μ chain) for the indicated times. The cell lysates were subjected to immunoprecipitation with anti-CD22 antibody (Cy34.1). The precipitated proteins were immunoblotted with antiphosphotyrosine (pTyr) antibody (PT-66) and then reprobed with anti-CD22 polyclonal antibody. (E) In vitro hyperproliferation response of *Cmah*-null B cells to calcium signaling. Splenic B cells were assessed for proliferation using tetradecanoyl phorbol acetate (10 ng/ml) plus ionomycin (5 μg/ml) as stimulating reagents. The proliferation assay was performed as described in the legend of Fig. 6C. The open column represents the mean proliferation of wild-type B cells, and the filled column represents the mean proliferation of *Cmah*-null B cells. The bars represent the standard errors of the mean for triplicate cultures. +/+, wild type; −/−, *Cmah* null; IP, immunoprecipitation.

could be an important event to modulate B-cell activation in vivo.

Loss of Neu5Gc in relation to human deficiency for the *CMAH* gene. *Homo sapiens* is the sole mammalian species that lacks Neu5Gc expression throughout the body; indeed, Neu5Gc is antigenic to humans (31). This is a striking dif- ference between humans and chimpanzees, which express Neu5Gc as the major species of Sia throughout their bodies. Recently, it was shown that, unlike gene expression in the extant great apes, the *CMAH* gene is inactivated in humans (6, 22). Here, we demonstrated that Cmah is the sole enzyme responsible for the production of Neu5Gc in cells since our mouse model reproduced the human-like deficiency in Neu5Gc biosynthesis. This result confirmed that a genetic mu-

tation in the human lineage caused the lack of Neu5Gc in humans.

Sia is commonly used in the host recognition system of microbes, and human-specific microbes are reported to recog- nize epitope(s) containing Neu5Ac on human cells. The mouse described here is thus the first mammalian line that could be used as an animal model system to assess Sia-targeted human infectious diseases (15).

REFERENCES

1. Alizadeh, A. A., M. B. Eisen, R. E. Davis, C. Ma, I. S. Lossos, A. Rosenwald, J. C. Boldrick, H. Sabet, T. Tran, X. Yu, J. I. Powell, L. Yang, G. E. Marti, T. Moore, J. Hudson, Jr., L. Lu, D. B. Lewis, R. Tibshirani, G. Sherlock, W. C. Chan, T. C. Greiner, D. D. Weisenburger, J. O. Armitage, R. Warnke, R. Levy, W. Wilson, M. R. Grever, J. C. Byrd, D. Botstein, P. O. Brown, and L. M. Staudt. 2000. Distinct types of diffuse large B-cell lymphoma identified by gene expression profiling. Nature 403:503–511.
2. Baum, L. G., K. Derbin, N. L. Perillo, T. Wu, M. Pang, and C. Uittenbogaart. 1996. Characterization of terminal sialic acid linkages on human thymocytes. Correlation between lectin-binding phenotype and sialyltransferase expression. J. Biol. Chem. 271:10793–10799.
3. Blixt, O., B. E. Collins, I. M. Van Den Nieuwenhof, P. R. Crocker, and J. C. Paulson. 2003. Sialoside specificity of the Siglec family assessed using novel multivalent probes: identification of potent inhibitors of myelin associated glycoproteins. J. Biol. Chem. 278:31007–31019.
4. Buhl, A. M., and J. C. Cambier. 1997. Co-receptor and accessory regulation of B-cell antigen receptor signal transduction. Immunol. Rev. 160:127–138.
5. Cervenak, L., A. Magyar, R. Boja, and G. Laszlo. 2001. Differential expression of GL7 activation antigen on bone marrow B cell subpopulations and peripheral B cells. Immunol. Lett. 78:89–96.
6. Chou, H. H., H. Takematsu, S. Diaz, J. Iber, E. Nickerson, K. L. Wright, E. A. Muchmore, D. L. Nelson, S. T. Warren, and A. Varki. 1998. A mutation in human CMP-sialic acid hydroxylase occurred after the Homo-Pan divergence. Proc. Natl. Acad. Sci. USA 95:11751–11756.
7. Clark, E. A. 1993. CD22, a B cell-specific receptor, mediates adhesion and signal transduction. J. Immunol. 150:4715–4718.
8. Coico, R. F., B. S. Bhogal, and G. J. Thorbecke. 1983. Relationship of germinal centers in lymphoid tissue to immunologic memory. VI. Transfer of B cell memory with lymph node cells fractionated according to their receptors for peanut agglutinin. J. Immunol. 131:2254–2257.
9. Crocker, P. R. 2002. Siglecs: sialic-acid-binding immunoglobulin-like lectins in cell-cell interactions and signalling. Curr. Opin. Struct. Biol. 12:609–615.
10. Crocker, P. R., S. Kelm, C. Dubois, B. Martin, A. S. McWilliam, D. M. Shotton, J. C. Paulson, and S. Gordon. 1991. Purification and properties of sialoadhesin, a sialic acid-binding receptor of murine tissue macrophages. EMBO J. 10:1661–1669.
11. Crocker, P. R., and A. Varki. 2001. Siglecs in the immune system. Immunology 103:137–145.
12. Crocker, P. R., and A. Varki. 2001. Siglecs, sialic acids and innate immunity. Trends Immunol. 22:337–342.
13. Cyster, J. G., and C. C. Goodnow. 1997. Tuning antigen receptor signaling by CD22: Integrating cues from antigens and the microenvironment. Immunity 6:509–517.
14. Ellies, L. G., D. Ditto, G. G. Levy, M. Wahrenbrock, D. Ginsburg, A. Varki, D. T. Le, and J. D. Marth. 2002. Sialyltransferase ST3Gal-IV operates as a dominant modifier of hemostasis by concealing asialoglycoprotein receptor ligands. Proc. Natl. Acad. Sci. USA 99:10042–10047.
15. Gagneux, P., and A. Varki. 1999. Evolutionary considerations in relating oligosaccharide diversity to biological function. Glycobiology 9:747–755.
16. Han, H., D. J. Bearss, L. W. Browne, R. Calaluce, R. B. Nagle, and D. D. Von Hoff. 2002. Identification of differentially expressed genes in pancreatic cancer cells using cDNA microarray. Cancer Res. 62:2890–2896.
17. Han, S., S. R. Dillon, B. Zheng, M. Shimoda, M. S. Schlissel, and G. Kelsoe. 1997. V(D)J recombinase activity in a subset of germinal center B lymphocytes. Science 278:301–305.
18. Han, S., B. Zheng, D. G. Schatz, E. Spanopoulou, and G. Kelsoe. 1996. Neoteny in lymphocytes: Rag1 and Rag2 expression in germinal center B cells. Science 274:2094–2097.
19. Hathcock, K. S., C. E. Pucillo, G. Laszlo, L. Lai, and R. J. Hodes. 1995. Analysis of thymic subpopulations expressing the activation antigen GL7: expression, genetics, and function. J. Immunol. 155:4575–4581.
20. Hennet, T., D. Chui, J. C. Paulson, and J. D. Marth. 1998. Immune regulation by the ST6Gal sialyltransferase. Proc. Natl. Acad. Sci. USA 95:4504–4509.
21. Hokazono, Y., T. Adachi, M. Wabl, N. Tada, T. Amagasa, and T. Tsubata. 2003. Inhibitory coreceptors activated by antigens but not by anti-Ig heavy chain antibodies install requirement of costimulation through CD40 for survival and proliferation of B cells. J. Immunol. 171:1835–1843.
22. Irie, A., S. Koyama, Y. Kozutsumi, T. Kawasaki, and A. Suzuki. 1998. The molecular basis for the absence of N-glycolylneuraminic acid in humans. J. Biol. Chem. 273:15866–15871.
23. Itohara, S., P. Mombaerts, J. Lafaille, J. Iacomini, A. Nelson, A. R. Clarke, M. L. Hooper, A. Farr, and S. Tonegawa. 1993. T cell receptor delta gene mutant mice: independent generation of alpha beta T cells and programmed rearrangements of gamma delta TCR genes. Cell 72:337–348.
24. Kawano, T., S. Koyama, H. Takematsu, Y. Kozutsumi, H. Kawasaki, S. Kawashima, T. Kawasaki, and A. Suzuki. 1995. Molecular cloning of cyti-

25. Kawano, T., Y. Kozutsumi, T. Kawasaki, and A. Suzuki. 1994. Biosynthesis of N-glycolylneuraminic acid-containing glycoconjugates. Purification and characterization of the key enzyme of the cytidine monophospho-N-acetyl-neuraminic acid hydroxylation system. J. Biol. Chem. 269:9024–9029.
26. Kelm, S., A. Pelz, R. Schauer, M. T. Filbin, S. Tang, M. E. de Bellard, R. L. Schnaar, J. A. Mahoney, A. Hartnell, P. Bradfield, et al. 1994. Sialoadhesin, myelin-associated glycoprotein and CD22 define a new family of sialic acid-dependent adhesion molecules of the immunoglobulin superfamily. Curr. Biol 4:965–972.
27. Koyama, S., T. Yamaji, H. Takematsu, T. Kawano, Y. Kozutsumi, A. Suzuki, and T. Kawasaki. 1996. A naturally occurring 46-amino-acid deletion of cytidine monophospho-N-acetylneuraminic acid hydroxylase leads to a change in the intracellular distribution of the protein. Glycoconj. J. 13:353–358.
28. Laszlo, G., K. S. Hathcock, H. B. Dickler, and R. J. Hodes. 1993. Characterization of a novel cell-surface molecule expressed on subpopulations of activated T and B cells. J. Immunol. 150:5252–5262.
29. Lossos, I. S., A. A. Alizadeh, M. B. Eisen, W. C. Chan, P. O. Brown, D. Botstein, L. M. Staudt, and R. Levy. 2000. Ongoing immunoglobulin somatic mutation in germinal center B cell-like but not in activated B cell-like diffuse large cell lymphomas. Proc. Natl. Acad. Sci. USA 97:10209–10213.
30. MacLennan, I. C. 1994. Germinal centers. Annu. Rev. Immunol. 12:117–139.
31. Martin, M. J., A. Muotri, F. Gage, and A. Varki. 2005. Human embryonic stem cells express an immunogenic nonhuman sialic acid. Nat. Med. 11:228–232.
32. McHeyzer-Williams, L. J., M. Cool, and M. G. McHeyzer-Williams. 2000. Antigen-specific B cell memory: expression and replenishment of a novel B220⁻ memory B cell compartment. J. Exp. Med. 191:1149–1166.
33. McHeyzer-Williams, L. J., D. J. Driver, and M. G. McHeyzer-Williams. 2001. Germinal center reaction. Curr. Opin. Hematol. 8:52–59.
34. Mills, D. M., J. C. Stolpa, and J. C. Cambier. 2004. Cognate B cell signaling via MHC class II: differential regulation of B cell antigen receptor and MHC class II/Ig-αβ signaling by CD22. J. Immunol. 172:195–201.
35. Morita, S., T. Kojima, and T. Kitamura. 2000. Plat-E: an efficient and stable system for transient packaging of retroviruses. Gene Ther. 7:1063–1066.
36. Muchmore, E. A., M. Milewski, A. Varki, and S. Diaz. 1989. Biosynthesis of N-glycolylneuraminic acid. The primary site of hydroxylation of N-acetyl-neuraminic acid is the cytosolic sugar nucleotide pool. J. Biol. Chem. 264:20216–20223.
37. Muramatsu, M., V. S. Sankaranand, S. Anant, M. Sugai, K. Kinoshita, N. O. Davidson, and T. Honjo. 1999. Specific expression of activation-induced cytidine deaminase (AID), a novel member of the RNA-editing deaminase family in germinal center B cells. J. Biol. Chem. 274:18470–18476.
38. Murasawa, M., S. Okada, S. Obata, M. Hatano, H. Moriya, and T. Tokuhisa. 2002. GL7 defines the cycling stage of pre-B cells in murine bone marrow. Eur. J. Immunol. 32:291–298.
39. Nitschke, L. 2005. The role of CD22 and other inhibitory co-receptors in B-cell activation. Curr. Opin. Immunol. 17:290–297.
40. Novoradovskaya, N., M. L. Whitfield, L. S. Basehore, A. Novoradovsky, R. Pesich, J. Usary, M. Karaca, W. K. Wong, O. Aprelikova, M. Fero, C. M. Perou, D. Botstein, and J. Braman. 2004. Universal reference RNA as a standard for microarray experiments. BMC Genomics 5:20.
41. Pasare, C., and R. Medzhitov. 2005. Control of B-cell responses by Toll-like receptors. Nature 438:364–368.
42. Paulson, J. C., J. Weinstein, and A. Schauer. 1989. Tissue-specific expression of sialyltransferases. J. Biol. Chem. 264:10931–10934.
43. Poe, J. C., Y. Fujimoto, M. Hasegawa, K. M. Haas, A. S. Miller, I. G. Sanford, C. B. Bock, M. Fujimoto, and T. F. Tedder. 2004. CD22 regulates B lymphocyte function in vivo through both ligand-dependent and ligand-independent mechanisms. Nat. Immunol. 5:1078–1087.
44. Powell, L. D., and A. Varki. 1994. The oligosaccharide binding specificities of CD22 beta, a sialic acid-specific lectin of B cells. J. Biol. Chem. 269:10628–10636.
45. Razi, N., and A. Varki. 1998. Masking and unmasking of the sialic acid-binding lectin activity of CD22 (Siglec-2) on B lymphocytes. Proc. Natl. Acad. Sci. USA 95:7469–7474.
46. Reichert, R. A., W. M. Gallatin, I. L. Weissman, and E. C. Butcher. 1983. Germinal center B cells lack homing receptors necessary for normal lymphocyte recirculation. J. Exp. Med. 157:813–827.
47. Schauer, R. 1982. Sialic acids: chemistry, metabolism and function. Cell biology monographs, vol. 10. Springer-Verlag, New York, NY.
48. Schulte, R. J., M. A. Campbell, W. H. Fischer, and B. M. Sefton. 1992. Tyrosine phosphorylation of CD22 during B cell activation. Science 258:1001–1004.
49. Schwarzkopf, M., K. P. Knobeloch, E. Rohde, S. Hinderlich, N. Wiechens, L. Lucka, I. Horak, W. Reutter, and R. Horstkorte. 2002. Sialylation is essential for early development in mice. Proc. Natl. Acad. Sci. USA 99:5267–5270.
50. Sgroi, D., A. Varki, S. Braesch-Andersen, and I. Stamenkovic. 1993. CD22,

a B cell-specific immunoglobulin superfamily member, is a sialic acid-binding lectin. J. Biol. Chem. **268:**7011–7018.

51. **Shaffer, A. L., A. Rosenwald, E. M. Hurt, J. M. Giltnane, L. T. Lam, O. K. Pickeral, and L. M. Staudt.** 2001. Signatures of the immune response. Immunity **15:**375–385.

52. **Shapiro-Shelef, M., K. I. Lin, L. J. McHeyzer-Williams, J. Liao, M. G. McHeyzer-Williams, and K. Calame.** 2003. Blimp-1 is required for the formation of immunoglobulin secreting plasma cells and pre-plasma memory B cells. Immunity **19:**607–620.

53. **Shaw, L., and R. Schauer.** 1988. The biosynthesis of *N*-glycolylneuraminic acid occurs by hydroxylation of the CMP-glycoside of *N*-acetylneuraminic acid. Biol. Chem. Hoppe-Seyler **369:**477–486.

54. **Shaw, L., and R. Schauer.** 1989. Detection of CMP-*N*-acetylneuraminic acid hydroxylase activity in fractionated mouse liver. Biochem. J. **263:** 355–363.

55. **Shih, T. A., E. Meffre, M. Roederer, and M. C. Nussenzweig.** 2002. Role of BCR affinity in T cell dependent antibody responses in vivo. Nat. Immunol. **3:**570–575.

56. **Sjoberg, E. R., L. D. Powell, A. Klein, and A. Varki.** 1994. Natural ligands of the B cell adhesion molecule CD22 beta can be masked by 9-O-acetylation of sialic acids. J. Cell Biol. **126:**549–562.

57. **Takematsu, H., S. Diaz, A. Stoddart, Y. Zhang, and A. Varki.** 1999. Lysosomal and cytosolic sialic acid 9-*O*-acetylesterase activities can be encoded by one gene via differential usage of a signal peptide-encoding exon at the N terminus. J. Biol. Chem. **274:**25623–25631.

58. **Tedder, T. F., J. Tuscano, S. Sato, and J. H. Kehrl.** 1997. CD22, a B lymphocyte-specific adhesion molecule that regulates antigen receptor signaling. Annu. Rev. Immunol. **15:**481–504.

59. **Tsuji, S.** 1996. Molecular cloning and functional analysis of sialyltransferases. J. Biochem. (Tokyo) **120:**1–13.

60. **Varki, A.** 1992. Diversity in the sialic acids Glycobiology **2:**25–40. (Erratum, 2:168.)

61. **Varki, A.** 1997. Sialic acids as ligands in recognition phenomena. FASEB J. **11:**248–255.

62. **Varki, A., and T. Angata.** 2006 Siglecs—the major subfamily of I-type lectins. Glycobiology **16:**1R–27R.

63. **Wakabayashi, C., T. Adachi, J. Wienands, and T. Tsubata.** 2002. A distinct signaling pathway used by the IgG-containing B cell antigen receptor. Science **298:**2392–2395.

64. **Wuensch, S. A., R. Y. Huang, J. Ewing, X. Liang, and J. T. Lau.** 2000. Murine B cell differentiation is accompanied by programmed expression of multiple novel β-galactoside α2, 6-sialyltransferase mRNA forms. Glycobiology **10:** 67–75.

65. **Yamaji, T., T. Teranishi, M. S. Alphey, P. R. Crocker, and Y. Hashimoto.** 2002. A small region of the natural killer cell receptor, Siglec-7, is responsible for its preferred binding to α2,8-disialyl and branched α2,6-sialyl residues. A comparison with Siglec-9. J. Biol. Chem. **277:**6324–6332.

66. **Zhang, J., I. C. MacLennan, Y. J. Liu, and P. J. Lane.** 1988. Is rapid proliferation in B centroblasts linked to somatic mutation in memory B cell clones? Immunol. Lett. **18:**297–299.

Augmentation of drug-induced cell death by ER protein BRI3BP

Tetsuo Yamazaki [a,b,*], Nozomi Sasaki [a,b], Miyuki Nishi [b], Daiju Yamazaki [b],
Atsushi Ikeda [b], Yasushi Okuno [c], Shinji Komazaki [d], Hiroshi Takeshima [b]

[a] *The 21st Century Center of Excellence Program, Tohoku University Graduate School of Medicine, Sendai 980-8575, Japan*
[b] *Department of Biological Chemistry, Graduate School of Pharmaceutical Sciences, Kyoto University, Kyoto 606-8501, Japan*
[c] *Department of Genomic Drug Discovery Science, Graduate School of Pharmaceutical Sciences, Kyoto University, Kyoto 606-8501, Japan*
[d] *Department of Anatomy, Saitama Medical University, Saitama 350-0495, Japan*

Abstract

To determine the contribution of the endoplasmic reticulum (ER) to cell fate decision, we focused on BRI3-binding protein (BRI3BP) residing in this organelle. BRI3BP, when overexpressed, augmented the apoptosis of human embryonic kidney 293T cells challenged with drugs including the anti-cancer agent etoposide. In contrast, the knockdown of BRI3BP reduced the drug-triggered apoptosis. BRI3BP overexpression enhanced both mitochondrial cytochrome c release and caspase-3 activity in etoposide-treated cells. In response to etoposide, the ER reorganized into irregularly shaped lamellae in mock-transfected cells, whereas in BRI3BP-overexpressing cells, such reorganization was not observed. These observations suggest that BRI3BP is involved in the structural dynamics of the ER and affects mitochondrial viability. Taken together, BRI3BP, widely expressed in animal cell types, seems to possess a pro-apoptotic property and can potentiate drug-induced apoptosis.
© 2007 Elsevier Inc. All rights reserved.

Keywords: Apoptosis; Cytochrome c; Endoplasmic reticulum; Etoposide; BRI3BP; Mitochondria

The endoplasmic reticulum (ER) is a multifaceted organelle. It plays a major role in protein synthesis, folding and processing. In addition to its housekeeping functions, the ER emits signals to maintain cellular homeostasis. The accumulation of structurally defective proteins in the ER initiates stress responses, which are collectively referred to as the "unfolded protein response (UPR)" [1,2]. By enhancing the ERs capacity to refold and degrade aberrant proteins, the UPR initially operates in favor of cellular survival. In contrast, cell death is induced by the UPR when the cells are exposed to excessive and prolonged ER stress. The importance of the stress response has been demonstrated also in the pathogenesis of various diseases including ischemic/reperfusion injury, neurodegenerative diseases

and diabetes [3]. Toward a better understanding of such pathophysiological signals, it is necessary to identify and characterize the signaling proteins transmitting ER information to the cytoplasm.

In this work, we focused on an ER-resident protein, BRI3-binding protein (BRI3BP) [4,5]. On the basis of the results obtained, we propose that BRI3BP contributes to cell fate decision by mediating joint activities between the ER and mitochondria.

Methods

Transfection and pharmacological treatment. Human embryonic kidney 293T (293T) cells were grown in DMEM (WAKO, Tokyo, Japan) supplemented with 10% fetal calf serum (FCS) at 37 °C in a 5% CO_2 humidified incubator. For overexpression, the cDNA fragment encoding human BRI3BP or murine calumin was PCR-generated and cloned in frame into the pcDNA4/myc-His vector (Invitrogen). The pcDNA4/myc-His/lacZ vector coding for β-galactosidase was obtained from Clontech Inc. The cells were plated 16 h prior to transfection in 12-well plates at

* Corresponding author. Address: Department of Biological Chemistry, Graduate School of Pharmaceutical Sciences, Kyoto University, Kyoto 606-8501, Japan. Fax: +81 75 753 4605.
E-mail address: yamazakt@pharm.kyoto-u.ac.jp (T. Yamazaki).

1 × 10⁵ cells per well. The expression construct was transfected into the cells using Lipofectamine 2000 (Invitrogen). At 30 h posttransfection, etoposide (Etop), thapsigargin (Tg), and tunicamycin (Tu) (all from WAKO) were added to the culture medium. The cells were incubated for a further 40 h and then examined flow cytometrically. For BRI3BP depletion, the following small interfering RNA (siRNA) duplex obtained from Dharmacon was transfected into 293T cells using X-tremeGENE siRNA transfection reagent (Roche): 5'-gcucuuggauguucuuggauu-3' and 5'-uccaagaacauccaagagcuu-3'. Depletion of BRI3BP mRNA was confirmed by reverse transcription polymerase chain reaction (RT-PCR) using cDNAs, synthesized with PrimeScript reverse transcriptase (Takara Bio, Shiga, Japan), as templates. The following primers were used: for BRI3BP, 5'-GCGTCGACACCATGGGCGCGCGCGCCTCAGGCGG GC-3' and 5'-GCGAATTCTACTTGTCCTTGGAGCGGTCCAGGC TC-3', and for β-actin, 5'-GCATTGCTGACAGGATGCAG-3' and 5'-CCTGCTTGCTGATCCACATC-3'. The siRNA-transfected cells were split onto another 12-well plate at 72 h posttransfection. After 16 h, the cells were chemically challenged as descried above and analyzed.

Cell viability and caspase-3 activity assay. Cell viability was determined as described previously [6]. To examine caspase-3 activation, the transfected cells were treated with either dimethyl sulfoxide (vehicle) or Etop in the presence or absence of the cell-permeable pan-caspase inhibitor Z-VAD-fmk (BD Bioscience). Subsequently, caspase-3 activity was measured by flow cytometry using the CaspGLOW fluorescein active capase-3 staining kit (Medical & Biological Lab., Nagano, Japan) according to the manufacturer's instructions.

Mitochondrial cytochrome c release and transmembrane potential. Mitochondrial cytochrome c content was measured as described previously [7], except that the secondary antibody used was coupled with Alexa Fluor 488 instead of phycoerythrin. For examining the mitochondrial membrane potential, pharmacologically treated 293T cells were incubated for 30 min with DMEM supplemented with 10% FCS and 1 μg/ml rhodamine 123 (Rh123) in a 5% CO_2 humidified incubator, washed with PBS, and subjected to flow cytometry.

Immunoblotting. For the immunoblotting of whole cell lysates, transfected 293T cells were lyzed at 24 h posttransfection in RIPA buffer (10 mM Tris–HCl (pH 7.6), 150 mM NaCl, 2 mM EDTA, 1% Triton X-100 and 1% sodium deoxycholate, protease inhibitor cocktail (Nacalai Tesque, Tokyo, Japan)). The antibodies against the following proteins were used: BAK, BAX, Bcl-2, Bcl-X_L and actin (Santa Cruz Biotech.), and GRP78 (Abcam). BRI3BP antiserum was produced by injecting rabbits with a glutathione S-transferase fusion protein containing amino acids 203–253 of murine BRI3BP.

Ultrastructural analysis. The pharmacologically treated cells were prepared for electron microscopy study as described previously [8].

Statistics. Statistical significance was evaluated using Student's t test unless otherwise mentioned.

Results

Facilitation of drug-induced apoptosis by BRI3BP overexpression

The localization of BRI3BP to both the ER and the nuclear membrane prompted us to explore the possibility that BRI3BP is involved in signaling from the ER. To this end, 293T cells transfected with human BRI3BP that was fused to the mycHis tag (Suppl. Fig. 1A and B) were incubated with apoptosis inducers including ER stressors such as Tg (sarcoplasmic/endoplasmic Ca^{2+}–ATPase inhibitor) and Tu (N-glycosylation inhibitor), and the chemotherapy drug Etop (topoisomerase II inhibitor). The cells were probed using a combination of fluorescein isothiocyanate-coupled Annexin V (Annexin V-FITC) and the

DNA-specific fluorochrome 7-amino-actinomycin D (7-AAD) to simultaneously determine phosphatidyl serine exposure and plasma membrane permeability by flow cytometry [9,10]. Subsequently, cell subsets undergoing early (Annexin V⁺/7-AAD⁻) and late (Annexin V⁺/7-AAD⁺) apoptosis were quantified (Suppl. Fig. 1C). BRI3BP transfection led to a 15–30% increase in apoptosis compared with mock transfection. On the other hand, no obvious effects of β-galactosidase (cytosolic protein) and calumin (ER transmembrane protein [6]) on apoptosis were detected (Suppl. Fig. 1D), suggesting that BRI3BP specifically enhances drug-initiated apoptosis. Increased vulnerability to the pharmacological insults was corroborated over a wide range of drug concentrations (Fig. 1A).

Reduction of drug-induced apoptosis by BRI3BP depletion

We further investigated the role of BRI3BP using an siRNA-mediated knockdown approach. Transfection of an siRNA duplex corresponding to the BRI3BP open reading frame, but not to a scrambled (Sc) sequence, resulted in a marked decrease in the levels of BRI3BP mRNA and protein, as shown by RT-PCR and immunoblotting,
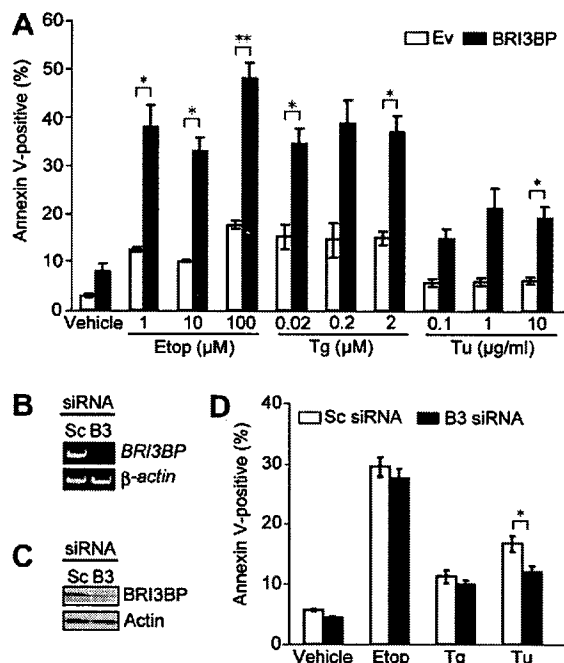

Fig. 1. Enhancement of drug-induced apoptosis by BRI3BP. (A) 293T cells transfected with either an empty vector (Ev) or the plasmid encoding the mycHis-tagged BRI3BP (BRI3BP) were pharmacologically treated for flow cytometric analysis. Annexin V positivity indicates the total percentage of two subpopulations (Annexin V⁺/7-AAD⁻ and Annexin V⁺/7-AAD⁺). The result represents mean ± SEM of five separate experiments. *P < 0.05, **P < 0.01. (B,C) 293T cells were transiently transfected with siRNA duplexes for either BRI3BP (B3) or an irrelevant sequence (Sc), followed by RT-PCR and immunoblotting. (D) The siRNA-transfected cells were challenged with the vehicle, 100 μM Etop, 2 μM Tg or 10 μg/ml Tu for flow cytometry. The result represents mean ± SEM of five independent experiments. *P < 0.05.

respectively (Fig. 1B and C). Tu-induced apoptosis was mitigated by BRI3BP depletion (Fig. 1D). On the other hand, apoptosis triggered by either Etop or Tg was marginally affected. Although the signaling pathways each drug utilizes for triggering apoptosis have not been elucidated in detail, death-signal cascades activated by Etop/Tg seem to be less BRI3BP-dependent than those activated by Tu. Taken together, the observed correlation between the abundance of BRI3BP and the vulnerability to pharmacological insults suggests that BRI3BP is involved in apoptosis-inducing signals emanating from the ER.

Enhanced activation of the caspase cascade by BRI3BP

We then investigated whether BRI3BP exploited the ordinary caspase signaling pathway [11] in enhancing the pharmacologically induced apoptosis of 293T cells. Because the pro-apoptotic property of BRI3BP became most clear upon treatment of the cells with Etop rather than with Tg or Tu, we analyzed the cells incubated with Etop with or without the cell-permeable pan-caspase inhibitor Z-VAD-fmk. Annexin V positivity determined by flow cytometry was decreased with Z-VAD-fmk, regardless of whether BRI3BP was transfected into the cells (Suppl. Fig. 2A). Correspondingly, the inhibitor reduced the activity of caspase-3, an effector caspase, in the Etop-treated cells as demonstrated by decreased signals derived from FITC-coupled DEVD-fmk, which irreversibly binds to activated caspase-3 (Suppl. Fig. 2B). The overexpression of BRI3BP, therefore, increases the sensitivity to Etop by upregulating the caspase cascade.

Mitochondrial damage induced by BRI3BP

The caspase-dependent facilitation of Etop-induced apoptosis by BRI3BP prompted us to examine which level along the caspase signaling pathway was modulated. The liberation of cytochrome c from the mitochondrial intermembrane space initiates apoptosome formation and culminates in the activation of effector caspases including caspase-3 [12,13]. Because chemotherapeutic agents trigger the mitochondrial release of cytochrome c, we hypothesized that this might be the step BRI3BP promoted in rendering the cells highly sensitive to Etop. The quantitation of mitochondrial cytochrome c content by flow cytometry revealed that BRI3BP overexpression induced an increase in the percentage of cytochrome c-negative subsets upon Etop treatment, indicating enhanced cytochrome c release (Fig. 2A). We further assessed the mitochondrial transmembrane potential ($\Delta\Psi_m$) using the membrane-permeable lipophilic cationic fluorochrome rhodamine 123 (Rh123) as a probe [9]. In response to Etop, BRI3BP-transfected cells showed $\Delta\Psi_m$ dissipation to a greater degree than mock-transfected control cells (Fig. 2B). Deterioration in mitochondrial functions, represented by both cytochrome c release and $\Delta\Psi_m$ collapse, is known to be closely associated with an imbalance between pro- and anti-apoptotic Bcl-2
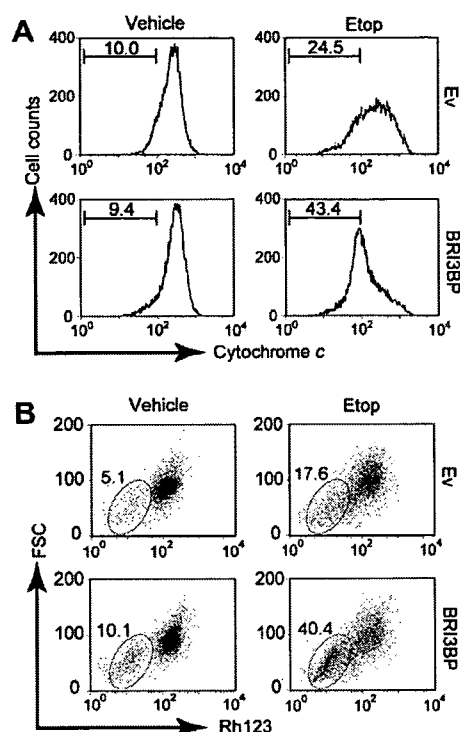

Fig. 2. Impairment of mitochondrial membrane integrity by BRI3BP overexpression. Transfected 293T cells challenged with 100 μM Etop were subjected to flow cytometric analysis of mitochondrial cytochrome c content (A) and transmembrane potential (B). FSC, forward light scatter. Experiments were repeated three times with similar results.

family members [14–16]. Immunoblot analysis detected no significant alterations in the expression levels of major Bcl-2 family proteins in BRI3BP-transfected cells (Suppl. Fig. 3), indicating that BRI3BP does not tip the balance, at least quantitatively, among the family members. Collectively, mitochondrial dysfunction underlies the priming of 293T cells by BRI3BP for Etop-induced apoptosis.

Absence of Etop-induced ER reorganization upon BRI3BP overexpression

Mitochondria lie adjacent to and operate in concert with the ER [17–19]. We then explored by electron microscopy the possibility that the mitochondrial dysfunction observed was secondary to the defects in the ER, where BRI3BP is localized. Treatment with the vehicle alone did not lead to a clear difference in ER morphology between mock- and BRI3BP-transfected 293T cells (Fig. 3A, B, E, and G). Upon exposure to Etop, the ER in the mock-transfected cells underwent morphological changes. It appeared in sections as whorls or a convoluted lamellar structure continuous with the nuclear membrane, to which mitochondria was frequently apposed (Fig. 3F). In contrast, such ER restructuring induced by Etop was effectively suppressed in the BRI3BP-overexpressing cells and the ER extending directly from the nuclear membrane was barely observed
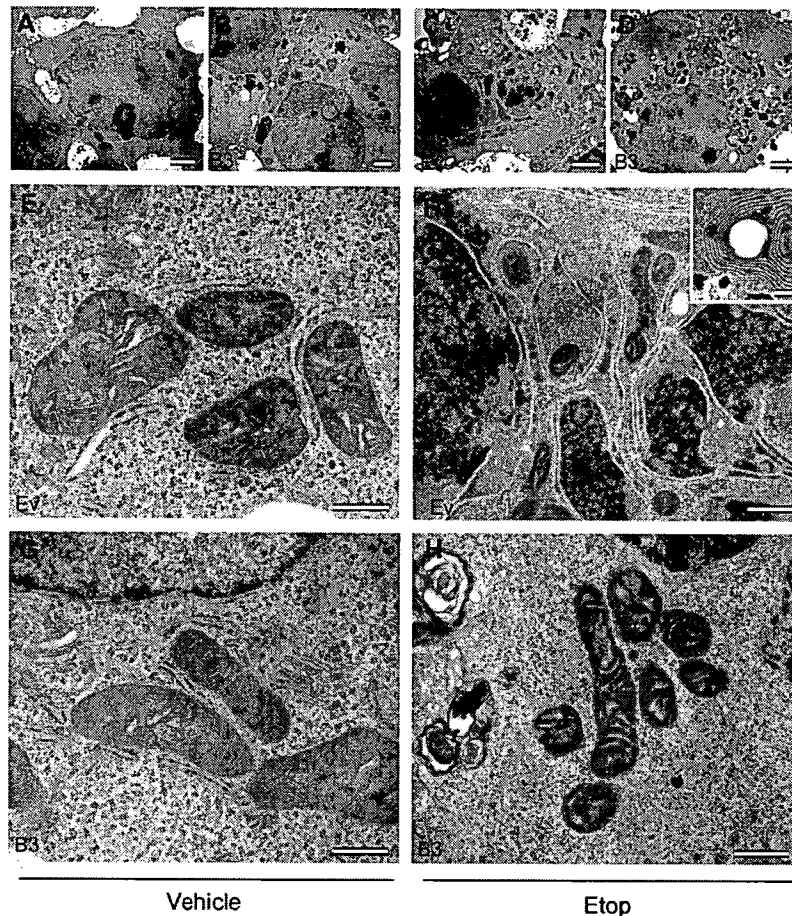
Vehicle	Etop

Fig. 3. Lack of ER transformation in BRI3BP-transfected 293T cells. The mock (Ev)- and the BRI3BP (B3)-transfected cells were treated with the vehicle (A, B, E, G) or 100 μM Etop (C, D, F, H) for electron microscopy. Bars, 2 μm (A–D); 0.5 μm (E–H). Data shown represent three separate experiments.

(Fig. 3H). In addition, structurally damaged mitochondria were more readily detected upon BRI3BP overexpression (Fig. 3C and D). These data suggest that the enforced expression of BRI3BP downregulates the structural plasticity of the ER, which is potentially linked to mitochondrial viability.

Discussion

In this report, we found that the BRI3BP transfection facilitates drug-induced apoptosis. It has been known that the overproduction of integral membrane proteins triggers the ER-overload response [20]. It is thus possible that the potentiation of pharmacologically induced apoptosis upon BRI3BP overexpression is attributable primarily to the excessive ER stress, but not to the specific action inherent to BRI3BP itself. However, this possibility is not supported by our data that GRP78, a chaperon induced by ER stress, was below the detection limit in both mock- and BRI3BP-transfected cells treated with either the vehicle or Etop (Suppl. Fig. 4). Therefore, in addition to BRI3BP overexpression, cofactors are required for facilitating apoptosis. This view is further supported by the fact that BRI3BP

transfection alone did not induce mitochondrial dysfunction (Fig. 2).

The ER elements have various morphological forms [21,22]. It is an attractive hypothesis that the structural shift of the ER could represent a cellular adaptive response that serves to minimize the propagation of cell death signals from the ER. Because the BRI3BP overexpression inhibited Etop-induced ER restructuring (Fig. 3), it can be assumed that the facilitation of Etop-triggered apoptosis is due to the impaired plasticity of ER morphology. Major protein components of the nuclear membrane undergo caspase-dependent proteolysis in Etop-challenged cells [23]. It is therefore hypothesized that the physiological functions of the nuclear membrane are severely perturbed in BRI3BP-overexpressing cells, which showed the enhanced caspase-3 activity in response to Etop. As a result, the ER, which is structurally continuous with the nuclear membrane, might be unable to reorganize in this setting.

In this report, the relationship between the BRI3BP level and cell survival/death was analyzed in vitro using a cell line challenged with apoptosis inducers. If this relationship holds true in vivo, a reduction or loss of BRI3BP might result in the inefficient elimination of harmful cells, favoring tumor development. The array-based analysis

has demonstrated that BRI3BP mRNA levels are lower in human tumor samples (Suppl. Fig. 5), suggesting the involvement of BRI3BP in cell fate decision under physiological conditions. It is therefore possible that the BRI3BP expression level is associated with pathogenesis and that BRI3BP is a potential target of pharmacological intervention.

Acknowledgments

Appendix A. Supplementary data

Supplementary data associated with this article can be found, in the online version, at doi:10.1016/j.bbrc.2007.08.082.

References

[1] R.J. Kaufman, Stress signaling from the lumen of the endoplasmic reticulum: coordination of gene transcriptional and translational controls, Genes Dev. 13 (1999) 1211–1233.

[2] D. Ron, P. Walter, Signal integration in the endoplasmic reticulum unfolded protein response, Nat. Rev. Mol. Cell Biol. 8 (2007) 519–529.

[3] C. Xu, B. Bailly-Maitre, J.C. Reed, Endoplasmic reticulum stress: cell life and death decisions, J. Clin. Invest. 115 (2005) 2656–2664.

[4] L. Lin, Y. Wu, C. Li, S. Zhao, Cloning, tissue expression pattern, and chromosome location of a novel human gene BRI3BP, Biochem. Genet. 39 (2001) 369–377.

[5] T. Katahira, Y. Imamura, D. Kitamura, The BASH/BLNK/SLP-65-associated protein BNAS1 regulates antigen-receptor signal transmission in B cells, Int. Immunol. 18 (2006) 545–553.

[6] M. Zhang, T. Yamazaki, M. Yazawa, S. Treves, M. Nishi, M. Murai, E. Shibata, F. Zorzato, H. Takeshima, Calumin, a novel Ca^{2+}-binding transmembrane protein on the endoplasmic reticulum, Cell Calcium 42 (2007) 83–90.

[7] N.J. Waterhouse, J.A. Trapani, A new quantitative assay for cytochrome *c* release in apoptotic cells, Cell Death Differ. 10 (2003) 853–855.

[8] H. Takeshima, S. Komazaki, K. Hirose, M. Nishi, T. Noda, M. Iino, Embryonic lethality and abnormal cardiac myocytes in mice lacking ryanodine receptor type 2, EMBO J. 17 (1998) 3309–3316.

[9] E. Bedner, X. Li, W. Gorczyca, M.R. Melamed, Z. Darzynkiewicz, Analysis of apoptosis by laser scanning cytometry, Cytometry 35 (1999) 181–195.

[10] I. Vermes, C. Haanen, C. Reutelingsperger, Flow cytometry of apoptotic cell death, J. Immunol. Methods 243 (2000) 167–190.

[11] I.N. Lavrik, A. Golks, P.H. Krammer, Caspases: pharmacological manipulation of cell death, J. Clin. Invest. 115 (2005) 2665–2672.

[12] D.R. Green, G. Kroemer, The pathophysiology of mitochondrial cell death, Science 305 (2004) 626–629.

[13] G. Kroemer, L. Galluzzi, C. Brenner, Mitochondrial membrane permeabilization in cell death, Physiol. Rev. 87 (2007) 99–163.

[14] J.M. Adams, Ways of dying: multiple pathways to apoptosis, Genes Dev. 17 (2003) 2481–2495.

[15] J.C. Reed, Proapoptotic multidomain Bcl-2/Bax-family proteins: mechanisms, physiological roles, and therapeutic opportunities, Cell Death Differ. 13 (2006) 1378–1386.

[16] M.F. van Delft, D.C.S. Huang, How the Bcl-2 family of proteins interact to regulate apoptosis, Cell Res. 16 (2006) 203–213.

[17] R. Rizzuto, P. Pinton, W. Carrington, F.S. Fay, K.E. Fogarty, L.M. Lifshitz, R.A. Tuft, T. Pozzan, Close contacts with the endoplasmic reticulum as determinants of mitochondrial Ca^{2+} responses, Science 280 (1998) 1763–1766.

[18] L. Scorrano, S.A. Oakes, J.T. Opferman, E.H. Cheng, M.D. Sorcinelli, T. Pozzan, S.J. Korsmeyer, BAX and BAK regulation of endoplasmic reticulum Ca^{2+}: a control point for apoptosis, Science 300 (2003) 135–139.

[19] G. Csordas, C. Renken, P. Varnai, L. Walter, D. Weaver, K.F. Buttle, T. Balla, C.A. Mannella, G. Hajnoczky, Structural and functional features and significance of the physical linkage between ER and mitochondria, J. Cell Biol. 174 (2006) 915–921.

[20] H.L. Pahl, P.A. Baeuerle, The ER-overload response: activation of NF-κB, Trends Biochem. Sci. 22 (1997) 63–67.

[21] C.M. Federovitch, D. Ron, R.Y. Hampton, The dynamic ER: experimental approaches and current questions, Curr. Opin. Cell Biol. 17 (2005) 409–414.

[22] N. Borgese, M. Francolini, E. Snapp, Endoplasmic reticulum architecture: structures in flux, Curr. Opin. Cell Biol. 18 (2006) 358–364.

[23] B. Buendia, A. Santa-Maria, J.C. Courvalin, Caspase-dependent proteolysis of integral and peripheral proteins of nuclear membranes and nuclear pore complex proteins during apoptosis, J. Cell Sci. 112 (1999) 1743–1753.

ELSEVIER

Abnormal features in mutant cerebellar Purkinje cells lacking junctophilins

Atsushi Ikeda [a,1], Taisuke Miyazaki [b,1], Sho Kakizawa [c], Yasushi Okuno [d],
Soken Tsuchiya [d], Akira Myomoto [d], Shin-ya Saito [e], Tetsuji Yamamoto [a],
Tetsuo Yamazaki [a], Masamitsu Iino [c], Gozoh Tsujimoto [d],
Masahiko Watanabe [b], Hiroshi Takeshima [a,e,*]

[a] Department of Biological Chemistry, Graduate School of Pharmaceutical Sciences, Kyoto University, Kyoto 606-8501, Japan
[b] Department of Anatomy, Hokkaido University Graduate School of Medicine, Sapporo, Japan
[c] Department of Pharmacology, Graduate School of Medicine, The University of Tokyo, Tokyo, Japan
[d] Department of Genomic Drug Discovery Science, Graduate School of Pharmaceutical Sciences, Kyoto University, Kyoto 606-8501, Japan
[e] Department of Medical Chemistry, Tohoku University Graduate School of Medicine, Sendai, Japan

Abstract

Junctional membrane complexes (JMCs) generated by junctophilins are required for Ca^{2+}-mediated communication between cell-surface and intracellular channels in excitable cells. Knockout mice lacking neural junctophilins (JP-DKO) show severe motor defects and irregular cerebellar plasticity due to abolished channel crosstalk in Purkinje cells (PCs). To precisely understand aberrations in JP-DKO mice, we further analyzed the mutant PCs. During the induction of cerebellar plasticity via electrical stimuli, JP-DKO PCs showed insufficient depolarizing responses. Immunochemistry detected mild impairment in synaptic maturation and hyperphosphorylation of protein kinase $C\gamma$ in JP-DKO PCs. Moreover, gene expression was slightly altered in the JP-DKO cerebellum. Therefore, the mutant PCs bear marginal but widespread abnormalities, all of which likely cause cerebellar motor defects in JP-DKO mice.
© 2007 Elsevier Inc. All rights reserved.

Keywords: Long-term depression; Multiple innervation; Protein kinase C; Ryanodine receptor

Functional communications between cell-surface and intracellular channels play indispensable roles in excitable cells [1]. Ca^{2+}-mediated channel crosstalk often takes place in specific subcellular structures, called the junctional membrane complexes (JMCs), which are characterized by close apposition of the endoplasmic/sarcoplasmic reticulum (ER/SR) and the cell membrane [2]. Of four junctophilin (JP) subtypes, JP1 and JP2 contribute to the formation of JMCs in striated muscle [3–5], while JP3 and JP4 are co-expressed in neuron [6]. Double-knockout mice deficient for both neural JPs (JP-DKO) exhibit impaired motor coordination and learning [7]. In cerebellar Purkinje cells (PCs), the generation of slow afterhyperpolarization (sAHP) following the climbing fiber (CF)-mediated complex spike requires Ca^{2+}-mediated channel crosstalk between P/Q-type voltage-gated Ca^{2+} channels (P/Q channels), ryanodine receptor channels (RyRs) and small-conductance Ca^{2+}-activated K^+ channels (SK channels). This channel communication probably occurs in JP-mediated JMCs and is indispensable for long-term depression (LTD) at parallel fiber (PF)-PC synapses. Indeed, this channel crosstalk is severely impaired and an LTD-inducing paradigm adversely leads to long-term potentiation

(LTP) in JP-DKO PCs [7]. In our continuing attempt to deepen understanding of impaired cerebellar functions in JP-DKO mice, we report irregular PC excitability, atypical CF-wiring to PCs, hyperphosphorylation of protein kinase C (PKC) and altered gene expression.

Materials and methods

Electrophysiological measurements. JP-3(−/−) JP-4(−/−) mice (JP-DKO) and JP-3(+/−) JP-4(+/−) mice (JP-DHE) were described previously [8]. For electrophysiological measurements, cerebellar slices were prepared from mice aged 8–10 weeks and whole-cell recordings were performed from PCs [7,9]. LTD was induced by conjunctive stimulation (CJS, 300 single PF stimuli in conjunction with single CF stimuli repeated at 1 Hz for 5 min) after the initial baseline recording for at least 10 min.

Morphological analysis. Morphological analyses were carried out using mice aged 6–10 weeks [10,11]. For anterograde labeling of CFs, the inferior olive in the anesthetized mice were injected with dextran Texas red. After 4 days of survival, mice were fixed by transcardial perfusion, and prepared microslicer sections were immunostained for calbindin and vesicular glutamate transporter type 2 (VGluT2) and analyzed using a confocal microscope.

Microarray, real-time PCR and immunoblot analyses. Total RNA was isolated from the cerebella of male mice aged 6–8 weeks using the Isogen reagent (Nippongene, Japan), fluorescence labeled and hybridized onto the Mouse Genome 430 2.0 Array (Affymetrix). Raw data obtained were analyzed as described previously [12]. Real-time PCR was performed using the Chromo 4 system (Bio-Rad). Cerebellar homogenates were examined by immunoblotting [10] using the following antibodies: total and phosphorylated (p) PKCγ, PDE (phosphodiesterase) 1C (Abcam), pPKCα, pMARCKS (myristoylated alanine-rich C kinase substrate), pNR1 (N-methyl-D-aspartate receptor 1), pGluR1 (glutamate receptor 1), pCREB (cAMP response element-binding protein), pDARPP (Dopamine- and cAMP-regulated neuronal phosphoprotein), Nab2 (Ngfi-A binding protein 2) (Millipore), pERK1/2 (extracellular signal-regulated kinase 1/2), Egr1 (early growth response 1) (Cell Signaling), β-tubulin (Sigma), and pCaMKII (Ca^{2+}/calmodulin-dependent protein kinase II, gift from Dr. Fukunaga, Tohoku University, Japan).

Results and discussion

Atypical depolarizing responses in JP-DKO PCs

In cerebellar slice preparations, CJS to both PF and CF induces LTD at PF-PC synapses [13]. In control mice, PF-evoked excitatory postsynaptic currents (PF-EPSCs) recorded in voltage-clamped PCs were remarkably decreased from the baseline level after CJS. As shown in Fig. 1A and B, this LTD-inducing paradigm adversely led to LTP in JP-DKO slices and control slices treated with apamin, an SK channel inhibitor. It has been reported that PF-LTP is induced by CJS when LTD was previously established at the CF-PC synapse [14] and also that both CF-evoked spikelets and dendritic Ca^{2+} transients are weakened in PCs after the induction of CF-LTD [15]. Based on these findings, we focused on CF-evoked spikelets in JP-DKO PCs. During CJS composed of stimuli repeated 300 times, control PCs showed constant voltage responses of spikelets, whereas spikelet numbers were significantly decreased at the late phase in both JP-DKO and apamin-treated control PCs (Fig. 1C and D). Therefore, the reverse plasticity in JP-DKO and the apamin-trea-
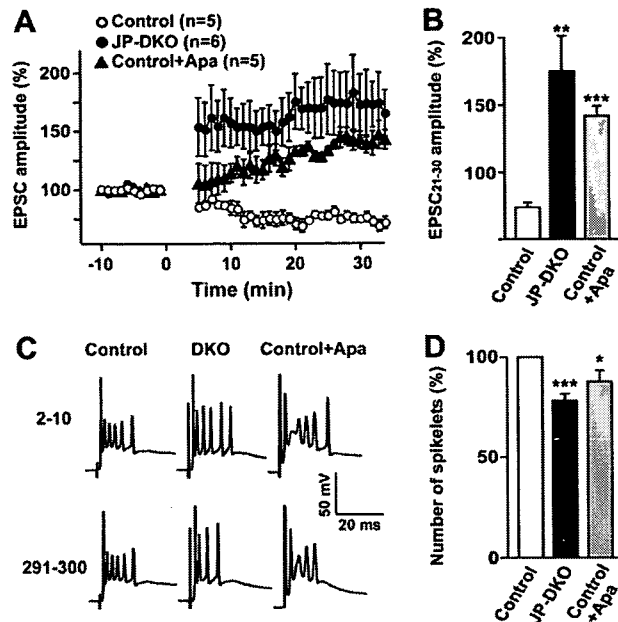

Fig. 1. Deformed spikelets during CJS in JP-DKO and apamin-treated control PCs. (A) PF-EPSCs were normalized by the mean value observed before CJS. Apamin (Apa; 200 nM) was applied to the bathing solution during recording. (B) Average EPSP amplitude during the 21–30 min period after CJS. (C) Representative voltage responses of PCs at early (2–10) and late (291–300) phases during CJS. (D) Averaged spikelet numbers at 291–300th responses normalized by values at 2–10th responses. Data are presented as means ± SEM ($*p < 0.05$, $**p < 0.01$ and $***p < 0.001$ in t-test).

ted PCs may be cardinally induced by the impaired spikelets due to insufficient SK channel opening.

In PCs, P/Q channels, rather than voltage-gated Na^+ channels, predominantly contribute to the generation of the slow spikelets [16]. JP-mediated channel crosstalk between P/Q channels, RyRs, and SK channels generates sAHP following spikelets [7]. Voltage-gated channels incorporate voltage-dependent inactivation features and their recovery from inactivated states requires the repolarization of the membrane potential. As a predicted mechanism underlying the reverse plasticity, sAHP deficiency may prevent the recovery of P/Q channels from the inactivated state and likely weakens spikelets during CJS in both JP-DKO and the apamin-treated PCs. JP-DKO and the apamin-treated PCs showed slight differences in the temporal profile of PF-EPSC potentiation (Fig. 1A). In particular, obvious differences observed immediately after CJS may imply as-yet-unrecognized defects in JP-DKO PCs besides sAHP deficiency due to SK channel dysfunctioning.

Mild disturbance in CF innervation to JP-DKO PCs

In our previous report, PF-PC synapses appeared normal in JP-DKO mice. To morphologically analyze the physical connection between CFs and PCs, CFs were anterogradely labeled (aCF) with dextran Texas red; CF-PC synapses and PC dendrites were visualized with antibodies

against VGluT2 and calbindin, respectively. In control mice (Fig. 2A), aCF precisely followed the branching of PC shaft dendrites and the terminal swellings of aCF overlapped completely with VGluT2. The DKO cerebellum showed no gross morphological abnormalities; PC dendrites were well branched and associated with CF terminals in regular spacing (Fig. 2B1). However, when carefully observed at higher magnifications, the same dendritic shaft innervated by aCF terminals (red arrows) was associated with a few synaptic terminals of tracer-unlabeled CFs (uCF, green arrows) (Fig. 2B2–5). This mild type of multiple CF innervation was often observed in the DKO cerebellum by this anatomical analysis, but was under the detection threshold by electrophysiological analysis [7].

In recent studies, a close correlation between multiple CF innervation and motor discoordination was repeatedly appreciated in a number of knockout mice including mutant mice defective in P/Q channels [11] and PKCγ [17]. Thus, the mild multiple innervation, together with the deranged Ca^{2+}-mediated channel crosstalk [7], may lead to severe motor discoordination in JP-DKO mice. The predominant distribution of JPs to the somatodendritic regions of PCs [6] suggests that PCs, rather than CFs, are likely responsible for the retention of the aberrant CF-PC

innervation in adult JP-DKO mice. Because both P/Q channels and PKCγ in PCs are essential for eliminating excess CF-PC synapses, two possibilities are reasonably proposed behind the mild symptom in JP-DKO PCs, i.e., the reduction of P/Q channel-mediated Ca^{2+} influx during repeated depolarization and the predicted hyperactivation of PKCγ (see below).

Hyperphosphorylation of PKCγ in JP-DKO PCs

Ca^{2+}-dependent signaling plays a central role for inducing synaptic plasticity such as cerebellar LTD and hippocampal LTP [13]. In our immunoblot analysis, the JP-DKO cerebellum showed an enhanced phosphorylation level at T674 of PKCγ without affecting other phosphorylation sites or its protein content (Fig. 3 and Suppl. Fig. 1). In addition, we did not detect any abnormalities in phosphorylation of well-known PKC substrates (MARCKS and NR1) or of other protein kinases. Since PKCγ is predominantly expressed in PCs among cerebellar cell types, the hyperphosphorylation seems to occur in JP-DKO PCs. Although we have observed regular CF-mediated Ca^{2+} responses in JP-DKO PC soma regions [7], sAHP deficiency could slightly prolong opening of P/Q channels upon sporadic stimuli. It might be that enhanced Ca^{2+} signaling at the microdomain level stimulates the autophosphorylation of PKCγ in JP-DKO PCs under basal conditions. In addition to facilitated autophosphorylation, PKCγ activation accompanies its translocation to the cell membrane from the cytoplasm. PKCγ was clearly detected in the cytoplasm and on the cell membrane, and no difference was observed in its subcellular localization between control and JP-DKO PCs (Suppl. Fig. 2). Although MARCKS and NR1 showed normal phosphorylation levels, it is still possible that PKCγ activity was enhanced to change phosphorylation states of unknown signaling molecules regulating cerebellar motor functions in JP-DKO PCs. On the other hand, PKCγ-knockout mice suffering severe multiple innervation have established its essential
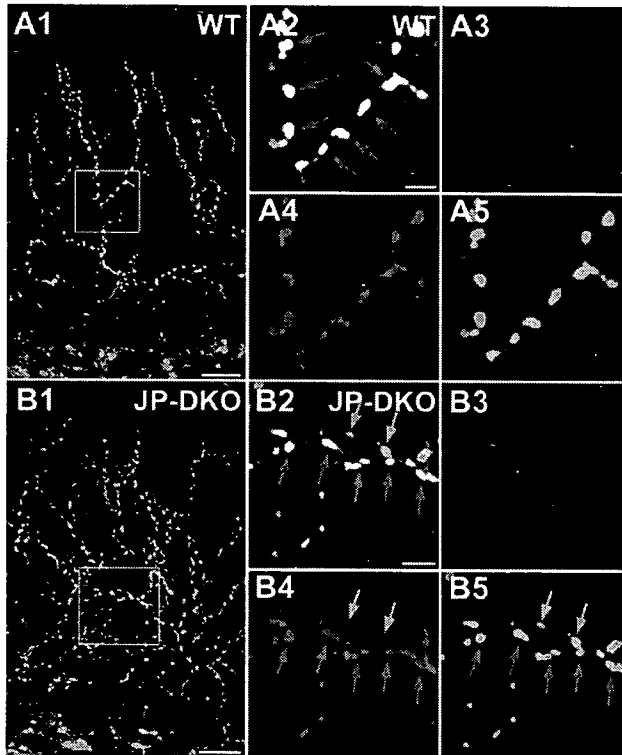

Fig. 2. Aberrant CF-PC innervation in JP-DKO cerebellum. Cerebellar sections were labeled for calbindin (blue), VGluT2 (green) and the anterograde CF tracer dextran Texas red (red) in control (A) and JP-DKO mice (B). Boxed regions in A1 and B1 are magnified in A2–5 and B2–5, respectively. The arrows indicate terminals of anterogradely-labeled CFs (aCF, red arrows) and unlabeled CFs (uCF, green arrows), respectively. Scale bars, 20 μm in A1 and B1; 5 μm in A2–5 and B2–5.
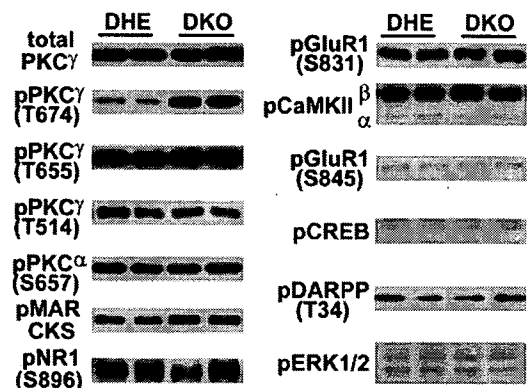

Fig. 3. Hyperphosphorylation at T674 of PKCγ in JP-DKO cerebellum. Representative immunoblot data are shown. The immunoreactivities were statistically analyzed in Suppl. Fig. 1.
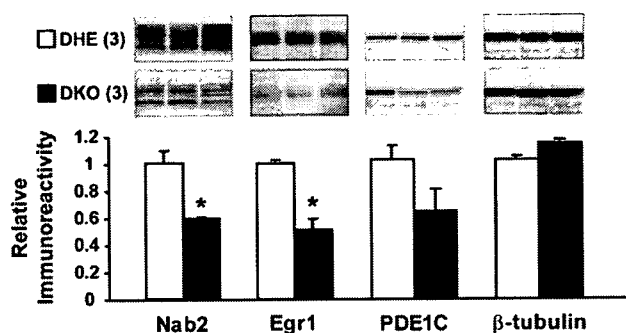
Fig. 4. Reduced expression of Nab2 and Egr1 in JP-DKO cerebellum. Immunoreactivities (upper images) were statistically analyzed. Data are presented as means ± SEM (n values in parentheses, $*p < 0.05$ in t-test).

role in CF-PC synaptic maturation [17]. Hyperphosphorylated PKCγ might also affect signaling processes for CF elimination in JP-DKO PCs.

Altered gene expression in JP-DKO cerebellum

We finally surveyed altered gene expression in the JP-DKO cerebellum. Our microarray analysis suggested minimally altered gene expression between genotypes (Suppl. Fig. 3), but identified eight up-regulated and three down-regulated candidate genes in JP-DKO mice (Suppl. Table 1). Of the candidates, the down-regulation of Nab2 was confirmed by real-time PCR and immunoblotting (Fig. 4 and Suppl. Fig. 4). Nab2 is a transcriptional corepressor induced by the zinc-finger transcription factor Egr1, which is up-regulated by neuronal stimuli and essential for LTP in hippocampal neurons [18]. In the JP-DKO cerebellum, Egr1 protein was obviously decreased (Fig. 4). The reduced Nab2 and Egr1 levels may be due to less electrically-active properties in JP-DKO PCs exhibiting the impaired spikelets (Fig. 1).

Although we need to examine the precise linkage between JP deficiency and several abnormalities reported here, they may be directly or indirectly connected with sAHP deficiency in JP-DKO PCs as discussed above. These chronic abnormalities observed under normal housing conditions likely further aggravate weakened spikelets caused by the sAHP deficiency to produce the severity of the reverse plasticity in the JP-DKO cerebellum. Our previous study suggests impairments of overall brain functions, including the salivary reflex and hippocampus-dependent memory in JP-DKO mice [8]. The presented data clearly suggest that JP-mediated JMCs are essential for a broad range of cellular homeostasis in various neurons.

Appendix A. Supplementary data

Supplementary data associated with this article can be found, in the online version, at doi:10.1016/j.bbrc. 2007.09.062.

References

[1] M.J. Berridge, M.D. Bootman, H.L. Roderick, Calcium signalling: dynamics, homeostasis and remodeling, Nat. Rev. Mol. Cell. Biol. 4 (2003) 517–529.

[2] A. Divet, S. Paesante, C. Bleunven, A. Anderson, S. Treves, F. Zorzato, Novel sarco(endo)plasmic reticulum proteins and calcium homeostasis in striated muscles, J. Muscle Res. Cell Motil. 26 (2005) 7–12.

[3] H. Takeshima, S. Komazaki, M. Nishi, M. Iino, K. Kangawa, Junctophilins: a novel family of junctional membrane complex proteins, Mol. Cell 6 (2000) 11–22.

[4] K. Ito, S. Komazaki, K. Sasamoto, M. Yoshida, M. Nishi, K. Kitamura, H. Takeshima, Deficiency of triad junction and contraction in mutant skeletal muscle lacking junctophilin type 1, J. Cell Biol. 154 (2001) 1059–1068.

[5] S. Komazaki, M. Nishi, H. Takeshima, Abnormal junctional membrane structures in cardiac myocytes expressing ectopic junctophilin type 1, FEBS Lett. 542 (2003) 69–73.

[6] M. Nishi, H. Sakagami, S. Komazaki, H. Kondo, H. Takeshima, Coexpression of junctophilin type 3 and type 4 in brain, Mol. Brain Res. 110 (2003) 102–110.

[7] S. Kakizawa, Y. Kishimoto, K. Hashimoto, T. Miyazaki, K. Furutani, H. Shimizu, M. Fukaya, M. Nishi, H. Sakagami, A. Ikeda, H. Kondo, M. Kano, M. Watanabe, M. Iino, H. Takeshima, Junctophilin-mediated channel crosstalk essential for cerebellar synaptic plasticity, EMBO J. 26 (2007) 1924–1933.

[8] S. Moriguchi, M. Nishi, S. Komazaki, H. Sakagami, T. Miyazaki, H. Masumiya, S. Saito, M. Watanabe, H. Kondo, H. Yawo, K. Fukunaga, H. Takeshima, Functional uncoupling between Ca^{2+} release and afterhyperpolarization in mutant hippocampal neurons lacking junctophilins, Proc. Natl. Acad. Sci. USA 103 (2006) 10811–10816.

[9] S. Kakizawa, T. Miyazaki, D. Yanagihara, M. Iino, M. Watanabe, M. Kano, Maintenance of presynaptic function by AMPA receptor-mediated excitatory postsynaptic activity in adult brain, Proc. Natl. Acad. Sci. USA 102 (2005) 19180–19185.

[10] T. Miyazaki, K. Hashimoto, A. Uda, H. Sakagami, Y. Nakamura, S. Saito, M. Nishi, H. Kume, A. Tohgo, I. Kaneko, H. Kondo, K. Fukunaga, M. Kano, M. Watanabe, H. Takeshima, Disturbance of cerebellar synaptic maturation in mutant mice lacking BSRPs, a novel brain-specific receptor-like protein family, FEBS Lett. 580 (2006) 4057–4064.

[11] T. Miyazaki, K. Hashimoto, H.S. Shin, M. Kano, M. Watanabe, P/Q-type Ca^{2+} channel alpha 1A regulates synaptic competition on developing cerebellar Purkinje cells, J. Neurosci. 24 (2004) 1734–1743.

[12] R.A. Irizarry, B.M. Bolstad, F. Collin, L.M. Cope, B. Hobbs, T.P. Speed, Summaries of Affymetrix GeneChip probe level data, Nucleic Acids Res. 31 (2003) e15.

[13] M. Ito, Cerebellar circuitry as a neuronal machine, Prog. Neurobiol. 78 (2006) 272–303.

[14] M. Coesmans, J.T. Weber, C.I. De Zeeuw, C. Hansel, Bidirectional parallel fiber plasticity in the cerebellum under climbing fiber control, Neuron 44 (2004) 691–700.

[15] J.T. Weber, C.I. De Zeeuw, D.J. Linden, C. Hansel, Long-term depression of climbing fiber-evoked calcium transients in

Purkinje cell dendrites, Proc. Natl. Acad. Sci. USA 100 (2003) 2878–2883.

[16] M.T. Schmolesky, J.T. Weber, C.I. De Zeeuw, C. Hansel, The making of a complex spike: ionic composition and plasticity, Annu. N. Y. Acad. Sci. 978 (2002) 359–390.

[17] M. Kano, K. Hashimoto, C. Chen, A. Abeliovich, A. Aiba, H. Kurihara, M. Watanabe, Y. Inoue, S. Tonegawa, Impaired synapse elimination during cerebellar development in PKCγ mutant mice, Cell 83 (1995) 1223–1231.

[18] M.W. Jones, M.L. Errington, P.J. French, A. Fine, T.V. Bliss, S. Garel, P. Charnay, B. Bozon, S. Laroche, S. Davis, A requirement for the immediate early gene Zif268 in the expression of late LTP and long-term memories, Nat. Neurosci. 4 (2001) 289–296.